Production of sustainable solid biofuel from waste and lignocellulosic biomass by hydrothermal carbonization

（水熱炭化による廃棄物とリグノセルロース系バイオマスからの持続可能な固体バイオ燃料の生産）

Hokkaido University　　Graduate School of Agriculture
Frontiers in Production Sciences　　Doctor Course

ALIYU Mohammed

Production of sustainable solid biofuel from waste and lignocellulosic biomass by hydrothermal carbonization

Thesis submitted to the Graduate School of Agriculture
Hokkaido University, Sapporo, Japan in partial fulfilment of the requirements for the award of the degree of Doctor of Philosophy (PhD) in Bioproduction Engineering
(Laboratory of Agricultural Biosystem Engineering)

ALIYU Mohammed

March, 2022

DECLARATION

I hereby declare that this Thesis titled: "Production of sustainable solid biofuel from waste and lignocellulosic biomass by hydrothermal carbonization" is a collection of my original research work and it has not been presented for any other qualification anywhere. Information from other sources (published or unpublished) has been duly acknowledged.

ALIYU Mohammed
Student number: 32195002
GRADUATE SCHOOL OF AGRICULTURE
HOKKAIDO UNIVERSITY, SAPPORO, JAPAN.

-------- ---
SIGNATURE/ DATE

DEDICATION

This Thesis is dedicated to Almighty Allah, my beloved late parents, my lovely wife, lovely children, and my siblings.

ACKNOWLEDGEMENTS

I will forever be grateful to my mentor and supervisor Prof. Iwabuchi Kazunori for his constructive criticism, advice, and guidance throughout the period of my research work. I sincerely appreciate all his effort. I would also like to thank the dissertation committee members, Prof. Koseki Shigenobu and Associate Prof. Shimizu Naoto for finding time to check my thesis.

I also wish to register my appreciation to Dr. Takanori Itoh for his guidance and support throughout my study. My acknowledgement will not be complete without appreciating my colleagues and friends in the laboratory of Agricultural and Biosystem Engineering, Hokkaido University, Sapporo, Japan for their cooperation throughout the program.

I also acknowledge the effort of my current Head of Department Engr. Dr. S. M. Dauda, the former Head of Department Engr. Prof. B. A. Adejumo, the former and present Deans of School of Infrastructure, Process Engineering and Technology (SIPET), Engr. Prof. O. K. Abubakre and Engr. Prof. Z. D. Osunde. I also acknowledge all my senior colleagues and my colleagues in the Department of Agricultural and Bioresources Engineering, Federal University of Technology, Minna for their unrelenting effort in the Department.

I also acknowledge and register my profound appreciation to the Tertiary Education Trust Fund (TETFund) of Nigeria and the Tanigurogumi Corporation Shiobara 1100, Japan for their financial support during the program.

Finally, my sincere gratitude goes to the Almighty Allah for sparing my life and giving me the wisdom and capability to be able to carry out this research work. I hereby say "Praise be to Allah, the lord of the worlds"

EXECUTIVE SUMMARY

Biomass as an energy source has high potential to replace fossil fuel due to its renewability and carbon neutral nature. However, to increase the energy density of biomass, it needs to be pre-treated. Hydrothermal carbonization (HTC) is one of the promising alternative techniques used for the pre-treatment of biomass. However, the requirement to submerge biomass in water to decompose it to form hydrochar in the HTC process usually results in large volume of the post-process liquid phase. The effective way on how to handle the large volume of the post-process water has remained a subject of discussion and a challenge to the full commercialization of HTC in an industrial scale. To contribute additional solution to this problem, this study investigated the feasibility of vapor-based HTC (V-HTC) using high biomass-to-water (B/W) ratio, which minimizes the water required. Dairy manure (DM) was hydrothermally treated at temperatures of 200, 230, 255 and 270 °C and B/W ratio of 0.1, 0.18, 0.25, 0.43, 0.67 and 1.0 representing liquid-based HTC (L-HTC) to V-HTC conditions for 20 minutes, then the produced hydrochars were characterized by calorific, proximate, ultimate and thermogravimetric analyses. The results showed that the mass yields of hydrochar decreased with increasing temperature but was essentially stable at high B/W ratios. Notably, the calorific values of the hydrochars increased with increasing temperature and B/W ratio, and the energy density increased by 46%. Due to the higher mass yield and increased energy density, maximum energy yields at each temperature (86.0–97.4%) were observed at a B/W ratio of 1.0. To further enhance the fuel properties of hydrochar, a co-hydrothermal carbonization (co-HTC) of dairy manure (DM) and wood shavings from *Larix kaempferi*, commonly known as the Japanese larch (JL) was investigated. The JL was mixed with the DM at 25, 50 and 75 wt.% ratios. Co-HTC was conducted at 260 °C for 20 minutes. The resulting hydrochars were characterised based on the physicochemical properties and the thermal behaviour. Results showed that the hydrochar solid biofuel properties improved as the ratio of JL was increased. The produced hydrochars were in the region of lignite and closed to the region of the coal with increased fixed carbon, carbon contents and lowered H/C and O/C ratios. Hydrochar with ash content of 7.2±0.5% was obtained at 75 wt.% JL. In addition, the higher heating value (HHV) of hydrochar increased remarkably to 26.4±0.02 MJ/kg as the mass ratio of the JL was increased.

TABLE OF CONTENTS

LIST OF TABLES

LIST OF FIGURES

THESIS STRUCTURE

The thesis is organized in five (5) chapters as follows:

- Chapter one (1) gives the background to the study, which includes problem identification and the objectives of the study.
- Chapter two (2) introduces some literature background for the study,
- Chapter three (3) presents the first phase of the study on the HTC of dairy manure.
- Chapter four (4) presents the second phase of the study on the co-hydrothermal carbonization (co-HTC) of the dairy manure and Japanese larch.
- Chapter five (5) gives the conclusion and recommendation for further study.

CHAPTER 1

1.0 INTRODUCTION

1.1 Background to the study

Biomass is composed of lignocellulosic material derived from the living organic materials such as wood and agricultural residues [1]. Biomass also includes non-lignocellulosic materials such as animal and municipal solid wastes [1]. Biomass is currently one of the major sources of renewable energy and has a promising potential to replace the fossil fuel [2, 3]. The growing concerns about the cost, depletion in availability, and negative environmental associated with the use of fossil fuels [2, 4] has made the production of energy from biomass imperative. The utilization of biomass as an energy source does contributes to the net effect of the greenhouse gases [3, 5]. An example of a waste biomass that is sustainable but underutilized to produce energy is the animal manure.

Waste biomass such as animal manure is increasingly gaining attention due to the fast-growing animal husbandry across the world [6]. For this reason, animal manure generation have been reported in billions of tons in some countries annually [6, 7]. In Hokkaido prefecture of Japan alone, about 20 million tons of animal manure is generated annually [8]. Hence, biomass from animal manure could become one of the sustainable sources of biofuel production [6, 9]. However, the direct use of biomass for energy purposes could result in low efficiency due to its heterogeneity, low bulk density, high moisture content, and low energy density. Hence, to improve the fuel properties of biomass, it needs to be pre-treated [10, 11].

One of available alternatives to pre-treat biomass is through hydrothermal carbonization (HTC). HTC is a thermochemical and effective technique for improving

the fuel properties of biomass as a solid biofuel source [6, 9, 12]. The conversion process uses hot compressed water at a moderate temperature range of 180 to 280 °C in an autoclave reactor [5, 11, 13]. Unlike other available thermal conversion technologies for biomass, HTC does not need the pre-drying of a feedstock before carbonization. Hence, saves the energy required for drying of a feedstock before conversion to a solid biofuel. The solid biofuel produced from HTC is referred to as hydrochar and has energy density close to the coal.

1.2 Problem identification

The use of water in HTC is very critical because it governs the decomposition of biomass to hydrochar by hydrolysis [14, 15]. Water serves as a solvent and catalyst during HTC pre-treatment of biomass [5, 13, 16]. However, the need to submerge biomass in large amount of water, which is a unique feature of HTC, would require proper wastewater treatment after the HTC process to remove dissolved organic acids and other compounds prior to discharge into the environment [13, 16, 17]. In most HTC studies, hydrochar is produced with much quantity of water which implies the use of low biomass to water ratio (B/W) where the feedstock is immersed in sufficient water to facilitate higher heat exchange between the feedstock and the liquid medium [9, 12, 18–20], but this tends to generate much post-process wastewater. The effective way on how to handle the large amount of the post-process water has remained a subject of discussion and a challenge to the full commercialization of HTC in an industrial scale. Attempts to address this include water recycling, recovery of dissolved organic chemicals, usage in anaerobic digestion processes, and wastewater treatment [21–26] but all add significant additional construction and operating costs to commercial scale operations. Also, the amount of the dissolved organic compounds recoverable is reported to minimal [21, 24, 25] coupled

with the fact that larger percentage of studies on HTC is majorly concentrated on the production of hydrochar [5, 16]. Therefore, this study considered a feasible and cost-effective way by increasing B/W ratio in the HTC process. To achieve this, the effect of increasing B/W ratio at different HTC process temperatures using animal manure was investigated in this study.

In addition, the solid biofuel produced from animal manure via HTC pre-treatment is recognized for its high ash content [7, 9, 12, 27, 28]. These high ash contents of the carbonized solid biofuel from animal manure could result in severe ash related problems such as fouling and scaling deposits if directly used for combustion [29]. Consequently, this can lead to a reduction in the available area for heat transfer in a furnace and some connecting sections of combustion equipment [30]. It is, therefore, imperative to consider a technique such as the co-hydrothermal carbonization (co-HTC) of animal manure with a low ash content lignocellulosic biomass that could further help to improve the fuel property and reduce the ash content for efficient utilization as a solid biofuel. Therefore, this study further conducted a co-HTC of DM and the Japanese larch (JL) using B/W ratio of 1.0.

1.3 Aim and objectives of the study

The aim of the study was to produce a solid biofuel from dairy manure and lignocellulosic biomass while the specific objectives of the study are:

1. To evaluate the effect of increasing biomass to water ratio (B/W) on the hydrochar mass yield and fuel properties of hydrochar from DM.

2. To conduct a co-HTC of the DM and JL at the B/W ratio of 1.0 (obtained as the best from the first objective of the study) due to the high ash content of the hydrochar from DM.

1.4 List of publications included in this thesis

- Improvement of the fuel properties of dairy manure by increasing the biomass-to-water ratio in hydrothermal carbonization. Submitted to *PLOS ONE SCIENTIFIC JOURNAL*.
- Upgrading the fuel properties of hydrochar by co-hydrothermal carbonization of dairy manure and Japanese larch (*Larix kaempferi*): product characterization, thermal behaviour, kinetics, and thermodynamic properties. Published in *biomass conversion and biorefinery*, springer nature.

CHAPTER 2

2.0 LITERATURE REVIEW

2.1 Biomass and its products

Biomass is derived from plant and animal and does not need millions of years to develop like the fossil fuel [1]. A key advantage of biomass over the fossil fuel is that it can reproduce, hence, it is considered a renewable source of energy. Biomass absorbs carbon dioxide (CO_2) from the atmosphere during its growth process through photosynthesis [3]. During the combustion of biomass, the absorbed CO_2 is released back to the atmosphere, hence biomass does not contribute net CO_2 to the atmosphere [1, 31]. This key property of biomass makes it carbon neutral.

2.2 Sources of biomass

The sources of biomass include tiny grasses, trees, and small to large animal wastes. Table 2.1 shows some biomass sources.

Table 2.1: biomass sources

Biomass type	Sub-type	Examples
Virgin biomass	Terrestrial biomass	i. Grasses ii. Energy crops iii. Cultivated crops iv. Forest residues
	Aquatic biomass	i. Water plant ii. Algae
Waste biomass	Municipal wastes	i. Municipal solid wastes ii. Biosolids, sewage iii. Landfill gas
	Agricultural solid wastes	i. Livestock and manure ii. Agricultural crop residues
	Forestry residues	i. Barks, leaves, floor residues
	Industrial wastes	i. Demolition wood, sawdust ii. Waste oil/fat

Source: [1]

2.3 Component and structure of biomass

Biomass is a complex mixture of organic materials such as carbohydrate, fat, oil, protein etc. The main component of biomass includes extractives, fiber components and ash [1,

32]. Extractives refers to substances present in vegetable or animal tissue that include protein, oil, starch, and sugar which can be separated by successive treatment with solvents and recovered by evaporating the solution [1]. The fiber provides structural strength to the plant which allows it to stand above the ground without support [1]. A typical cell wall is made of carbohydrates and lignin while carbohydrates are mainly cellulose or hemicellulose fibers, which gives strength to the plant structure, while the lignin holds the fibers together. Ash is the inorganic component of the biomass after complete combustion. Fig. 2.1 shows a typical lignocellulosic biomass structure and components.

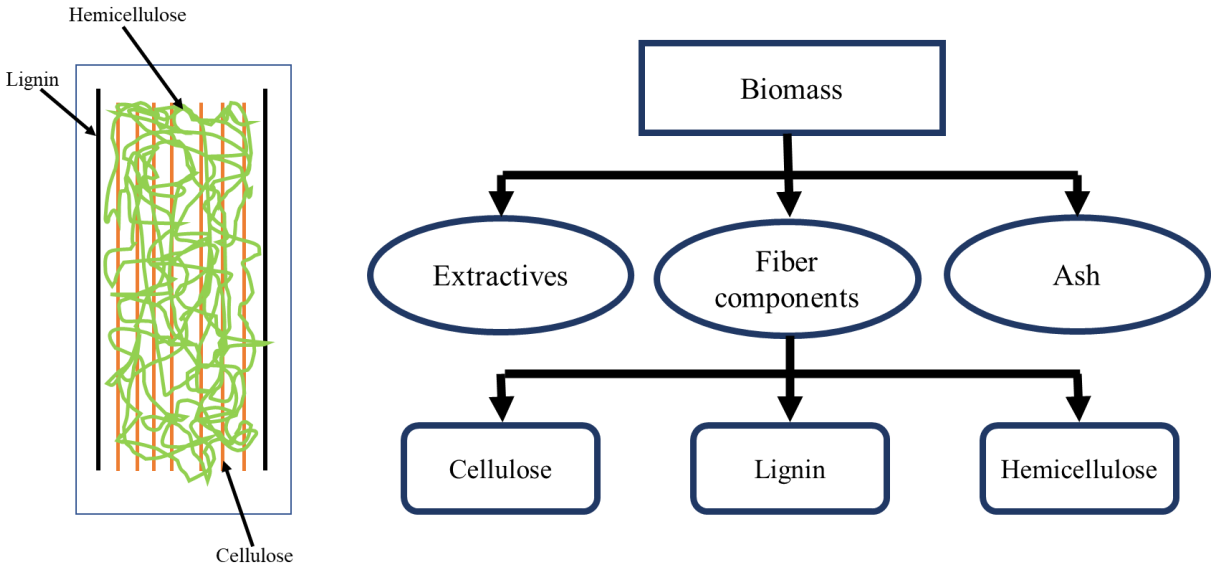

Fig. 2.1: A typical lignocellulosic biomass structure and components.

2.4 Biomass conversion techniques

Several methods are currently available for the conversion of biomass to a desired product for different application. These techniques include hydrothermal carbonization (HTC) or wet torrefaction, dry torrefaction, pyrolysis, gasification etc. These biomass pre-treatment methods are classified based on their operating condition [1]. The employment of these

methods most times depends on the desired product, feedstock type, moisture content of the feedstock etc. The Fig. 2.2 below shows some thermochemical conversion techniques for biomass to value added products.

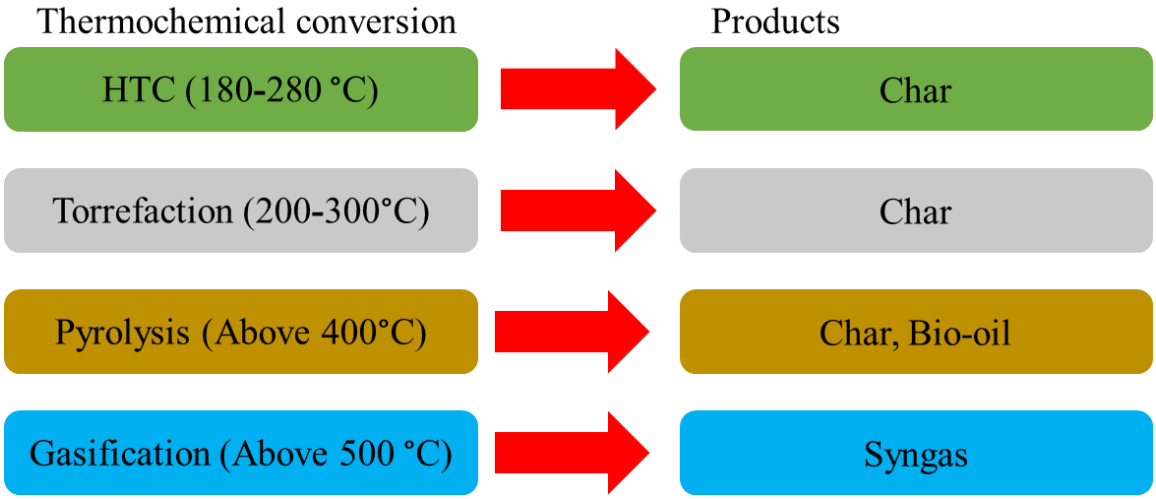

Fig. 2.2: Thermochemical conversion and products

2.4.1 Hydrothermal carbonization (HTC)

HTC also known as wet torrefaction is a thermochemical process for converting biomass to a high energy dense solid product. The conversion process uses hot compressed water at a moderate temperature range of 180 to 280 °C in an autoclave reactor [9]. The pressure in the reactor during the process is the range of 2 to 6 MPa and reaction time of 5 to 240 minutes [5]. The pressure rise in the reactor is autogenic (it is not controlled) depending on the process temperature. Unlike other available thermal conversion technologies for biomass, HTC can be used to convert high moisture content feedstock to a solid biofuel. Products from HTC include the solid biofuel referred to as hydrochar, process water and small amount of the gaseous products. A typical HTC process is illustrated in Fig. 2.3 below. Depending on the operation temperature and the desired product, the hydrothermal

process can be further classified as hydrothermal liquefaction (HTL) and hydrothermal gasification (HTG) or super-critical water gasification (SCWG) [5, 33]. The temperature range for HTL is reported to be between 250 – 400 °C [34] while HTG or SCWG is reported to be between 500 – 750 °C [35]. The desired end products of these two processes are liquid and gaseous fuel respectively.

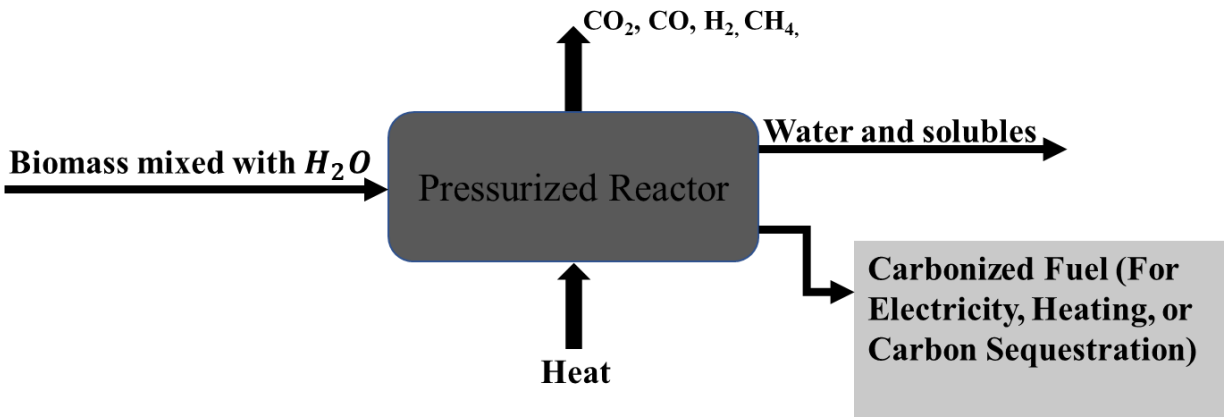

Fig. 2.3: A typical HTC process

2.4.1.1 Reaction mechanism in HTC

The reaction mechanism in HTC includes hydrolysis, dehydration, decarboxylation, polymerization, and aromatization [5, 15, 33]. These processes do not occur in a successive manner rather they occur simultaneously and are connected to each other [15]. Hydrolysis is the first step to be initiated and has the lowest activation energy [14, 15]. Hydrolysis breaks down the biomass chemical structure through the cleavage of the bonds of the bio-macromolecules with water molecules [14, 15, 36]. The hydrolysis process creates saccharides and some fragment of lignin in the liquid phase. Dehydration refers to the removal of water from the biomass matrix through the elimination of the hydroxyl group. Dehydration reaction in HTC covers both the physical and chemical processes. Chemical dehydration significantly lowers the H/C and O/C ratios [36]. Decarboxylation

is the removal of CO_2 and CO by the elimination of carboxyl and carbonyl groups [37] while aromatization occurs because of dehydration and decarboxylation processes [36].

2.4.2 Vapor-based and liquid-based HTC

Vapothermal carbonization (VTC) or the vapor-based HTC (V-HTC) involves the decomposition of biomass through the action of water vapor. B/W ratio can be used to differentiate HTC into liquid-based (L-HTC) and vapor-based (V-HTC) [19, 38, 39]. When the feedstock is submerged in water prior to carbonization, it is referred to L-HTC [19, 38]. When the feedstock is just in a moist condition or has no contact with bulk liquid water, it is often referred to as V-HTC [19]. A feedstock of high B/W ratio is used to conduct the V-HTC. Due to insufficient water in a feedstock of high B/W ratio, it is expected that the decomposition of biomass to hydrochar would be largely governed by vapor. However, V-HTC, is sometimes performed by placing a feedstock of high B/W ratio on a basket or a mesh few centimetres above the base of the reactor to avoid contact with water or the use of pipes to conduct steam to the biomass for decomposition [19, 39]. In this way, the reactor that is conventionally used for HTC needs to be modified before conducting the V-HTC.

The L-HTC has advantages such as greater effect of heat transfer between liquid and feedstock, higher carbon content and lower amount of ash contents [18]. Some notable benefits of conducting HTC with high B/W ratio or the V-HTC, include that; vapor can penetrate the biomass matrix at a faster rate due to its lower density compared to liquid, increased mass yield, increased fixed carbon, little or no mechanical dewatering is required after the process, avoidance of excessive use of water, eliminates post-process water handling and the heating value of the product could also increase [38].

2.4.3 Applications of hydrochar

Hydrochar has potential application for energy production, soil amendment/carbon sequestration, adsorbent for pollution control and remediation, medical application [16, 33] etc.

2.4.3.1 Hydrochar energy source

Hydrochar can be used as an alternative to coal for energy generation, since ash forming alkaline are mostly removed during HTC and increased its energy density, it therefore makes it suitable for direct usage as solid biofuel [5]. In addition, hydrochar can be used for the synthesis of fuel cells, batteries, and electrodes supercapacitors [15, 16].

2.4.3.2 Hydrochar for soil amendment/carbon sequestration

The use of hydrochar in soil amendment is related to nutrient release, mineralization, soil alteration, germination, growth of different crops, water retention [5, 40] etc. However, little information is available on the use of hydrochar for soil amendment. This could be due to its production process which is usually associated with organic acids and could be detrimental to plant growth [5].

2.4.4 Dry torrefaction

This is also known as mild pyrolysis and refers to a thermochemical process by which biomass is heated in an inert atmosphere at a process temperature range of 200 to 300 °C and a residence time of 30 minutes to several hours [5]. The degree of torrefaction depends on the temperature and the residence time to which it was subjected. A major objective of torrefaction is to increase the energy density of biomass by increasing its carbon content and at the same time reduce the oxygen content [41].

2.4.5 Pyrolysis

Pyrolysis is a thermochemical process is heated to an elevated temperature around 300 to 650 °C in the absence of oxygen [5]. The process results into three main products namely carbon-rich solid, bio-oil and non-condensable gases such as CO, CO_2, CH_4 and H_2. The process is sub-divided into slow, fast, flash and intermediate pyrolysis depending on the temperature, reaction time and heating rate [33].

2.4.6 Gasification

Gasification is a thermochemical conversion of biomass at high temperature range of 600 to 1200 °C for a short residence time. The major product of gasification is a mixture of gases known as syn gases [42]. Ideally, in gasification no solid biofuel is produced because most of the organic materials are converted to gases and ash. In practical term, small amount of solid is formed (mostly less than 10%) [1]. The small amount of the solid formed contains high concentration of alkaline and alkaline earth metal [5].

2.5 Solid fuel properties of biomass

2.5.1. Heating value

Heating value is one of the important indices of the fuel properties of biomass. It is the amount of heat energy released when a unit mass of a solid fuel is completely combusted and can be measured in terms of energy content per unit mass [1, 32]. This can be measured in terms of the higher heating value (HHV) with the inclusion of the heat of vaporization of water. HHV is also referred to as the gross calorific value (GCV) [32].

2.5.2 Proximate composition

Proximate analysis is used to express solid fuel components in terms of moisture content (M), volatile matter (VM), ash (ASH) content and fixed carbon (FC) [43]. The VM is the quantity of the condensable and non-condensable gases released when the fuel is heated [1]. The amount of the VM released depends on the heating temperature and the heating rate. The ASH content is the inorganic solid residue left after complete combustion of a solid fuel. The ASH content plays an important role in biomass utilization especially if it contains alkali metals (e.g., potassium or sodium) and halides (e.g., chlorine). These components in ASH can cause fouling and corrosion of combustion equipment and gasifiers [44]. The FC represents the solid carbon that remained after the subtraction of the M, VM and ASH. The FC include the elemental carbon and the carbonaceous residue formed in the process of heating during the VM determination [1].

2.5.3 Ultimate composition

The ultimate composition of biomass and solid fuel include the carbon (C), hydrogen (H), nitrogen (N), oxygen (O) and sulphur (S) contents [45]. These properties can be determined using an elemental analyzer. The measured values of these properties are sometimes used to estimate the HHV of the biomass and/or solid fuels [45, 46]. The carbon content is the most important property because it gives the indication of the energy value of a feedstock. The hydrogen content also contributes to the energy value of a feedstock but has less influence compared to the carbon content. The oxygen content is usually very high in raw biomass but can be reduced by pre-treatment. The reduction of oxygen in biomass increases its energy density [42]. The oxygen content is most times estimate indirectly by subtracting other elements from 100%. The nitrogen content in

biomass is low and hence, it does not have a significant contribution to the energy density of biomass or solid fuel. The sulphur content is also very low in biomass (less than 0.1%). It can contribute to the emission of toxic gases such as SO_2 during combustion.

2.6 Thermogravimetric analysis

Thermogravimetric analysis (TGA) is a useful technique for studying the thermal behaviour of a solid fuel [47, 48]. The TGA is used to observe the changes in mass of a solid fuel sample as a function of temperature or time of combustion. Depending on the environment or the gas employed in conducting the TGA (e.g., air atmosphere, oxygen, argon, nitrogen etc.), it can be used to study combustion process, pyrolysis, gasification of biomass or solid fuel [48]. Another useful application of the TGA is the study of the kinetics of biomass or solid fuel degradation [6, 49]. In addition, TGA is also useful to estimate the proximate compositions in biomass or solid fuel. The data generated from the TGA is used to plot the curves for the mass loss and the mass loss rates against the temperature. The mass loss rate is referred to as the differential thermogravimetric (DTG) data. The characteristic temperatures can be determined subsequently from the mass loss and mass loss rate curves.

2.7 Kinetics of solid fuel degradation

To design a combustion, pyrolysis, gasifier equipment etc. it is important to understand the thermal degradation behaviour and kinetics of biomass [2, 6, 50, 51]. Properties such as the activation energy, thermodynamic properties are useful in the study of biomass kinetics. The data generated from the TGA at different heating rates are used to fit established kinetic models [51]. Kinetic models such as the Flynn-Wall-Ozawa (FWO)

and Kissinger-Akahira-Sunose (KAS) are useful methods for determining the kinetic parameters of biomass or solid fuel decomposition [2, 49].

CHAPTER 3

Improvement of the fuel properties of dairy manure by increasing the biomass-to-water ratio in hydrothermal carbonization

Mohammed Aliyu[a,b], Kazunori Iwabuchi[c,*], Takanori Itoh[d]

[a] Graduate School of Agriculture, Hokkaido University, Kita 9, Nishi 9, Kita-ku, Sapporo, Hokkaido 060-8589, Japan

[b] Agricultural and Bioresources Engineering, Federal University of Technology, P. M. B. 65, Minna, Niger State, Nigeria

[c] Research Faculty of Agriculture, Hokkaido University, Kita 9, Nishi 9, Kita-ku, Sapporo, Hokkaido 060-8589, Japan

[d] Tanigurogumi Corporation, Shiobara 1100, Nasushiobara, Tochigi 329-2921, Japan

[*]Corresponding email: iwabuchi@bpe.agr.hokudai.ac.jp

ABSTRACT

There are many advantages to liquid-based hydrothermal carbonization (L-HTC) but the need to immerse the biomass in water generates more post-process water, hindering the commercialisation of HTC. To address this issue, this study investigated the feasibility of vapor-based HTC (V-HTC), which minimizes the water required. Dairy manure (DM) was hydrothermally treated at temperatures of 200, 230, 255 and 270 °C and biomass-to-water ratios (B/W) of 0.1, 0.18, 0.25, 0.43, 0.67 and 1.0 for 20 minutes, then the produced hydrochars were characterized by calorific, proximate, ultimate and thermogravimetric analyses. The results showed that the mass yields of hydrochar decreased with increasing temperature but was essentially stable at high B/W ratios. Notably, the calorific values of the hydrochars increased with increasing temperature and B/W ratio, and the energy density increased by 46%. Due to the higher mass yield and increased energy density, maximum energy yields at each temperature (86.0–97.4%) were observed at a B/W ratio of 1.0. The proximate and ultimate analyses revealed that the degree of coalification, such as the increase in carbon content and decrease in oxygen and volatile matter, progressed more under V-HTC than L-HTC conditions, likely because the lower liquid content in V-HTC facilitates the formation of secondary char and increases the reaction severity due to higher acidity. This study showed a potential approach for upgrading a semi-solid-state biomass by V-HTC.

Key words: Dairy manure, Biomass/water ratio, Thermochemical conversion, Hydrothermal carbonization, Vapothermal carbonization, Hydrochar, Solid biofuel

1.0 INTRODUCTION

The consumption of fossil fuels as energy sources has raised many global concerns due to their negative impact on the environment, such as greenhouse gas emissions [4, 52]. The utilization of biomass as an alternative energy source is thus imperative due to its carbon-neutral nature, but biomass typically must be pre-treated for efficient use as a solid biofuel [5]. Hydrothermal carbonization (HTC) is a biomass pre-treatment technique with low energy consumption and is an effective thermochemical technique for converting biomass into value-added carbon-rich products [5, 16]. The solid product generated from HTC is usually referred to as hydrochar. Hydrochar has enormous potential application in energy generation, and thus much research has focused on the production of high-quality hydrochar using HTC [5, 15, 16, 38, 53, 54].

Compared to other available thermal conversion technologies for biomass, HTC is better suited for converting biomass with high moisture content, such as livestock manure, because it uses moderately hot compressed water between 180 to 280 °C in an autoclave reactor [9, 16, 27, 55, 56]. However, the need to use water, which is a unique feature of HTC, requires proper wastewater treatment after the HTC process to remove dissolved organic acids and other compounds prior to discharge into the environment [5, 16]. In particular, in the most commonly used HTC process, called liquid-based HTC (L-HTC), the feedstock is immersed in sufficient water to facilitate higher heat exchange between the feedstock and the liquid medium, [18, 19] but this tends to generate more post-process wastewater [38]. Attempts to address this include water recycling, recovery of dissolved organic chemicals, usage in anaerobic digestion processes, and wastewater

treatment, [5, 17, 37, 57–59] but all add significant additional construction and operating costs to commercial scale operations.

To address these issues, the present study considers the feasibility of vapor-based HTC (V-HTC), which is easily achieved by increasing the biomass-to-water (B/W) ratio. The feedstock is moist or has no contact with bulk liquid water [18, 19]. Instead, biomass decomposition is mainly governed by water vapor, which can penetrate the biomass matrix faster due to its lower density compared to liquid [38]. V-HTC thus holds promise to simplify the handling of post-process water by avoiding excessive water usage prior to HTC treatment and/or requiring little mechanical dewatering after HTC treatment while improving fuel properties similar to that achieved by L-HTC.

The transition from L-HTC to V-HTC by varying the B/W ratio implies that the heat transfer medium leading to biomass decomposition is either liquid, vapor, or a mixture of the two [60]. Thus, the fuel properties of hydrochar are likely influenced by the B/W ratio but there is little direct evidence. For example, several studies have shown that the B/W ratio has little effect on mass and energy yields, [61, 62] whereas other studies have found that increasing the B/W ratio in HTC increases the mass yield and calorific value of hydrochar [63–65]. More importantly, to our knowledge, there are no published studies on HTC for B/W ratios above 0.67. Thus, HTC using feedstock with a moisture content below 60 wt.% (corresponding to a B/W ratio above 0.67) may be of limited utility, or perhaps water must be added to perform HTC. However, the moisture content of feedstock varies greatly depending on the situation and can be below 60 wt.% in some cases,[56] and thus HTC using a B/W ratio above 0.67 deserves investigation. HTC is conducted in a tightly closed system, ensuring that the generated vapor is in

continuous contact with the feedstock, allowing hydrochar production at higher B/W ratios. The authors therefore proposed the following hypothesis: hydrochar with improved fuel properties can be produced from low moisture content biomass without requiring the addition of more water. To verify this hypothesis, dairy manure (DM) as a test feedstock was hydrothermally treated at B/W ratios of 0.1, 0.18, 0.25, 0.43, 0.67 and 1.0, the calorific values were measured, and proximate, ultimate and thermogravimetric analyses were conducted to evaluate the fuel properties of the resulting hydrochars.

2.0 MATERIALS AND METHODS

2.1 Materials.

The DM used as a test material was obtained from an experimental farm at the Field Science Centre for Northern Biosphere, Hokkaido University, Japan. The sample was dried in an electric oven for 24 hours at 105 °C to a constant mass, then crushed using a mortar and pestle to reduce the particle size for ease of storage in a sealed Ziploc plastic bag [55, 66]. The sample was stored prior to the experiment.

2.2 Classification of the HTC process by the degree of saturation.

There is no clear definition of the classification state of HTC and thus the present study used the degree of saturation (S_r [%]), which is the ratio of water to the void fraction on a volumetric base, to classify four HTC states: complete L-HTC ($S_r = 100\%$), predominance of L-HTC ($67\% \leq S_r < 100\%$), mixture of liquid and vapor ($33\% \leq S_r < 67\%$), and predominance of V-HTC ($0\% \leq S_r < 33\%$). Even samples classified

as predominance of L-HTC or V-HTC likely involve the action of vapor or liquid to some extent, respectively. S_r was calculated using equation (1):

$$S_r = \frac{V_w}{V_a + V_w} \times 100 \quad (1)$$

where V_w (m^3) and V_a (m^3) are the volumes of water and air, respectively, and were determined using equations (2) and (3):

$$V_w = \frac{m_w}{\rho_w} \quad (2)$$

$$V_a = V - V_w - \frac{m_b}{\rho_b} \quad (3)$$

Here, m_w (kg) and ρ_w (kg/m^3) are the mass and specific density of water; V (m^3) is the apparent volume of the prepared sample in the reactor; and m_b (kg) and ρ_b (kg/m^3) are the dry mass and specific density of DM, respectively. Note that the specific density of DM (ρ_b) was determined to be 1.9 using a pycnometer at room temperature.

2.3 HTC reactor set-up and procedure.

Experiments were performed in a 70 mL stainless steel TVS-N2 (Taiatsu Techno, Tokyo, Japan) batch reactor (Figure 1) with a temperature and pressure limit of 300 °C and 8 MPa.

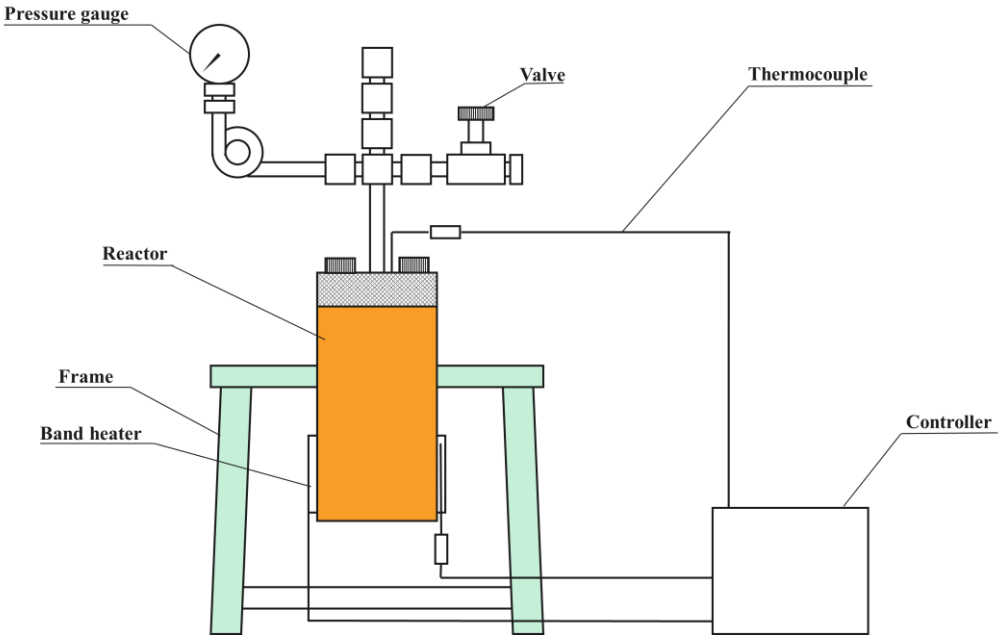

Figure 1: Schematic of the carbonization reactor used in this study.

Raw feedstocks were prepared by mixing about 5 to 20 ± 0.01 g of oven-dried sample and 20 to 45 ± 0.01 g of deionized water to obtain the desired B/W ratio with high accuracy (equation [4]).

$$\text{B/W ratio} = \frac{m_{\text{b}}}{m_{\text{w}}} \quad (4)$$

For each batch experiment, prepared raw feedstock was placed in the reactor and sealed, then flushed three times with pure nitrogen to remove oxygen. The process temperature range was 200 to 270 °C and the holding time was 20 minutes. A PID controller was used to achieve the desired temperature. The process was initiated at atmospheric pressure, and the average pressure (autogenic) rise in the reactor ranged from 1.5 to 6.2 MPa. After terminating the reaction, the reactor was placed in cold water for rapid cooling. The hydrochar was recovered from the reactor and dried to a constant mass

in an electric oven at 105 °C for 24 hours. The dried solid was milled, sieved, and stored in sample bottles for analyses.

A total of 24 experiments were conducted using four temperatures (200, 230, 255 and 270 °C) and six B/W ratios (0.1, 0.18, 0.25, 0.43, 0.67 and 1.0.). A holding time of 20 minutes at peak temperature was used to minimize further mass loss. Each experiment was conducted in triplicate.

2.4 Analyses

The mass yield of hydrochar (MY [%]), the energy densification ratio (EDR [-]), and the energy yield (EY [%]) were calculated using equations (5) to (7):

$$MY = \frac{m_{\mathrm{hc}}}{m_{\mathrm{b}}} \times 100 \quad (5)$$

$$EDR = \frac{HHV_{\mathrm{hc}}}{HHV_{\mathrm{b}}} \quad (6)$$

$$EY = MY \times EDF \quad (7)$$

where m_{hc} (kg) is the dry mass of the hydrochar, and HHV_{hc} (MJ/kg) and HHV_{b} (MJ/kg) are the higher heating values of the hydrochar and raw DM. The calorific values were determined using an OSK 200 bomb calorimeter (Ogawa Sampling, Saitama, Japan) by combusting at least 0.5 g of each sample in the calorimeter [67].

The ash content of each sample was determined using an electric muffle furnace (FUL220FA, ADVANTEC, Japan) by incinerating 1 g of oven-dried sample at 600 °C for 3 hours. The volatile matter (VM) was determined using ASTM standard procedure E872 by heating the samples at 950 °C for 7 minutes in an electric furnace. Then, the

fixed carbon (FC [%] = 100 − VM [%] − ash [%]) and the fuel ratio (FR [-] = FC/VM) were calculated.

The carbon, hydrogen and nitrogen content of the samples was determined using a CE-440 elemental analyser (Exeter Analytical, North Chelmsford, MA, USA). The oxygen content was calculated by difference (O [%] = 100 − C [%] − H [%] − N [%] − ash [%]). The percentage mass loss in carbon ($m_{\mathrm{c,loss}}$ [%]) and oxygen content ($m_{\mathrm{o,loss}}$ [%]) were calculated using equation (8) by considering the absolute initial and final masses of the raw sample ($m_{i,\mathrm{b}}$[kg]) and the produced hydrochars ($m_{i,\mathrm{hc}}$ [kg]).

$$m_{i,\mathrm{loss}} = \frac{m_{i,\mathrm{b}} - m_{i,\mathrm{hc}}}{m_{i,\mathrm{b}}} \times 100 \ (i = \text{carbon or oxygen}) \quad (8)$$

The combustion experiment was carried out using a thermal gravimetric analyser (TGA/DSC 1, Star System, Mettler Toledo, USA) under an air atmosphere. About 20 mg of sample was placed in an Al_2O_3 crucible and heated from 32 to 900 °C with an air flow rate of 100 mL/min at a heating rate of 10 °C/min. For each sample, the TGA experiment was repeated at least twice for accuracy [6]. The thermogravimetric (TG) and differential thermogravimetric (DTG) data were used to determine the following combustion parameters: ignition temperature (T_i [°C]), burnout temperature (T_b [°C]), burn out time (B_t [min]), residual mass (R_m [%]), maximum mass loss rate (DTG_m [%/min]) and its corresponding temperature (T_m [°C]). T_i indicates the temperature at which the fuel starts to burn while T_b denotes the temperature for complete combustion of the fuel; both were determined by the TG-DTG tangent method [6, 48]. T_m is the temperature at the maximum mass loss rate (DTG) or the peak temperature. The comprehensive combustion

index (*CCI* [min^{-2} $°C^{-3}$]) and the combustion stability index (*CSI* [min^{-1} $°C^{-2}$]) were calculated using equations (9) and (10), respectively [6, 68, 69].

$$CCI = \frac{DTG_{\mathrm{m}} \times DTG_{\mathrm{av}}}{T_{\mathrm{i}}^2 \times T_{\mathrm{b}}} \tag{9}$$

$$CSI = 8.5875 \times 10^7 \times \frac{DTG_{\mathrm{m}}}{T_{\mathrm{i}} \times T_{\mathrm{m}}} \tag{10}$$

3.0 RESULTS AND DISCUSSION

3.1 Classification of the HTC process by the degree of saturation.

Figure 2 shows the degree of saturation (S_r) based on the B/W ratio at initial conditions. According to the definition described in the Methods section, the HTC processes at each B/W ratio were predominantly complete for L-HTC at B/W ratios of 0.1 and 0.18, for L-HTC at a B/W ratio of 0.25, for a mixture of vapor and liquid phase at a B/W ratio of 0.43, and for V-HTC at B/W ratios of 0.67 and 1.0. At B/W ratios of 0.1 and 0.18 the raw feedstock was pasty but little leaching of gravitational water from the prepared feedstock was observed. When the B/W ratio of the feedstock was further increased, the liquid-like properties of the feedstock changed to a plastic-like state at a B/W ratio of 0.43 and then to a semi-solid state at B/W ratios of 0.67 and 1.0. The determination of the degree of saturation and visual observation during feedstock preparation suggest an increase in the free air space where water vapor could easily penetrate the feedstock at higher B/W ratios.

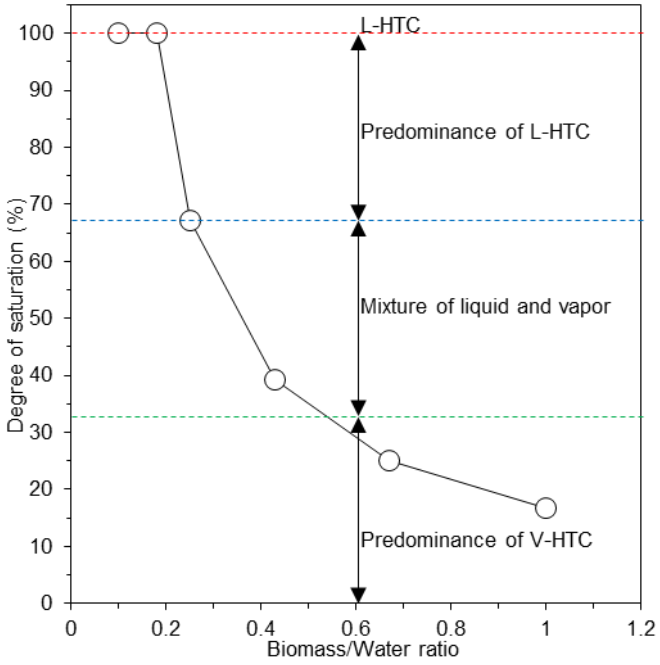

Figure 2: Classification of the HTC process based on the B/W ratio.

3.2 Effect of B/W ratio and temperature on mass distribution

Hydrochar products mass distribution at various B/W ratio up to 1.0 at various temperatures are shown in Figure 3. The mass distribution results indicate that the process conditions had effect on the product distribution due to increasing B/W ratio. Gaseous product generation increased as the B/W ratio was increased. The results in Figure 3 also indicate that higher amount of the gaseous product can be produced at higher B/W ratio in the process. Furthermore, hydrochars samples produced at B/W ratios of 0.43, 0.67 and 1.0 by V-HTC would have a higher production capacity than those produced at L-HTC conditions. The result also supports the result of the mass yield which showed that higher mass would be obtained at higher B/W ratios. Despite the increased reaction severity at higher temperatures, the yield of hydrochar can be maintained at higher temperatures of 255 °C and 270 °C.

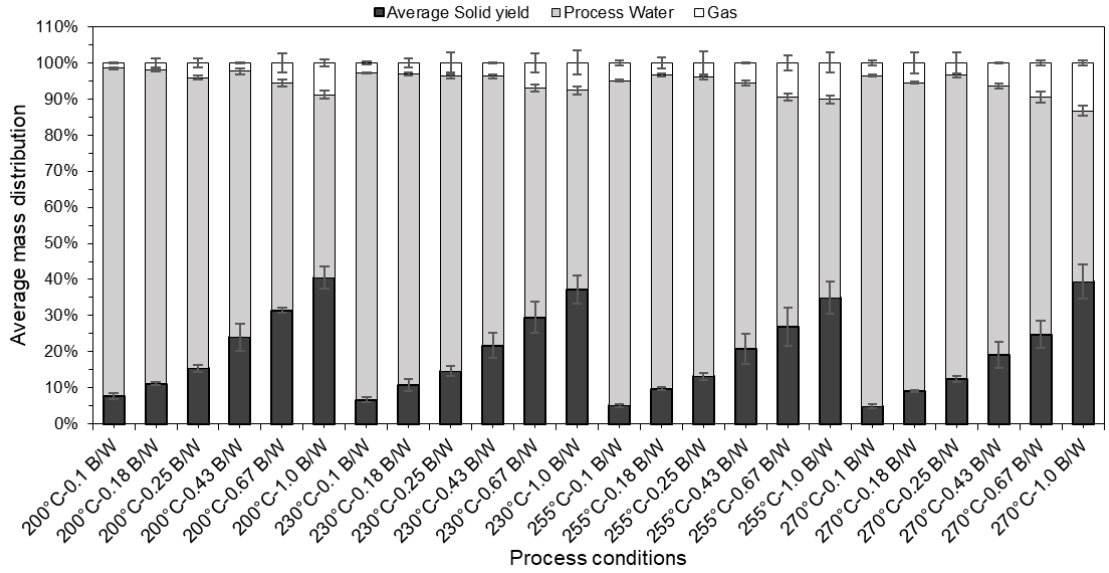

Figure 3: Average mass distribution at the different process conditions

3.3 Mass yield

Figure 4 shows the mass yield of hydrochar prepared at different temperatures and B/W ratios. The mass yields decreased with increasing process temperature. The mass yields showed only small fluctuations regardless of the B/W ratio. The mass yield in a thermochemical process indicates reaction severity, and thus higher temperature promotes biomass decomposition accompanied by the elimination of carboxyl, carbonyl and hydroxyl groups, producing CO_2, CO and H_2O [70, 71]. At 255 and 270 °C, the mass yield above a B/W ratio of 0.18 was higher than that at a B/W ratio of 0.1, due to either (i) the reaction severity decreasing above a B/W ratio of 0.18, resulting in higher mass yield, or (ii) the mass yield increasing due to physical deposition or chemical bonding of degraded substances on the hydrochar surface, although the reaction severity remains essentially stable above a B/W ratio of 0.18. Explanation (i) is based on liquid being superior to vapor for decomposing biomass, while explanation (ii) assumes there is little difference between each medium for decomposition, but degraded substances dissolved

in the liquid phase are more likely to contact the hydrochar surface due to the higher B/W ratio. Previous studies suggest that the polymerization of dissolved substances in the liquid phase and subsequent precipitation of insoluble solid substances on the hydrochar are more prevalent at higher B/W ratios, thereby increasing mass yield [16, 37, 59, 63, 72]. Furthermore, proximate and ultimate analyses revealed that DM is exposed to a more severe reaction at higher B/W ratios (discussed below in Table 1). Given these considerations, the authors conclude that explanation (ii) is more likely.

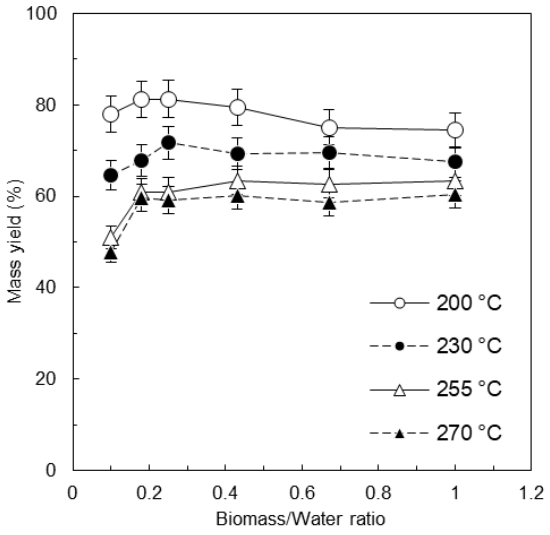

Figure 4: Mass yields at different B/W ratios and process temperatures.

3.4 Energy analyses

The higher heating value (HHV) of hydrochar increased from 17.2 to 25.1 MJ/kg as the B/W ratio and process temperature increased (Figure 5a). Higher temperatures increase hydrolysis, decarboxylation, dehydration, aromatization and re-condensation reactions, increasing the HHV of hydrochars [15, 27, 64]. The HHV showed upward trends with increasing B/W ratio, consistent with previous studies [18, 38, 63]. Given that

deposition or bonding of degraded substances on the hydrochar surface increases at higher B/W ratios, as described in the previous section, these substances likely contribute to increasing the HHV of hydrochars. Indeed, Volpe and Fiori [63] found that a higher B/W ratio in the HTC of olive waste promotes the formation of secondary char, which has a relatively high carbon content, on the produced hydrochar, although the study used lower B/W ratios of 0.08 to 0.25 compared to the present study. Kambo et al. [17] reported that the recirculation of HTC process water, rich in organic acids (acetic, formic, levulinic and glycolic acid) due to biomass degradation, improves the HHV of hydrochar. Therefore, the increased severity of the reaction may be another reason for the increase in HHV, since the acid concentration is likely higher and the acidity higher in V-HTC (Figure 6), where the liquid content is lower.

The EDR was calculated to evaluate the degree of energy densification due to the process. As expected, the EDR trend was similar to that of the HHVs, with a maximum EDR of 1.46 observed at 270 °C at a B/W ratio of 0.67 and at 270 °C and a B/W ratio of 1.0 (Table 1). The use of V-HTC with increasing B/W ratio may achieve more effective energy densification compared to L-HTC. Previous studies conducting the HTC of DM at 240 °C at a B/W ratio of 0.05 for 4 hours observed EDRs of 1.27 and 1.37, respectively [9, 27]. In contrast, the present study achieved an EDR of 1.37 at a lower temperature of 230 °C and a shorter holding time of 20 minutes using a higher B/W ratio of 1.0.

The EY increased as the B/W ratio was increased across the process temperatures but decreased with increasing process temperature (Figure 5b). In general, there is a negative correlation between the mass yield and the EDR: as the reaction severity increases, the mass yield decreases and the calorific value increases. The present study

found that the EY increased with an increase in the B/W ratio, due to the mass yield not changing significantly while the HHV increased with increasing B/W ratio (Figures 4 and 5a). Accordingly, the energy analysis indicates that V-HTC with a high B/W ratio has both a higher hydrochar production capacity (kg m^{-3} s^{-1}) than L-HTC and can produce higher quality solid biofuel, a great advantage of V-HTC.

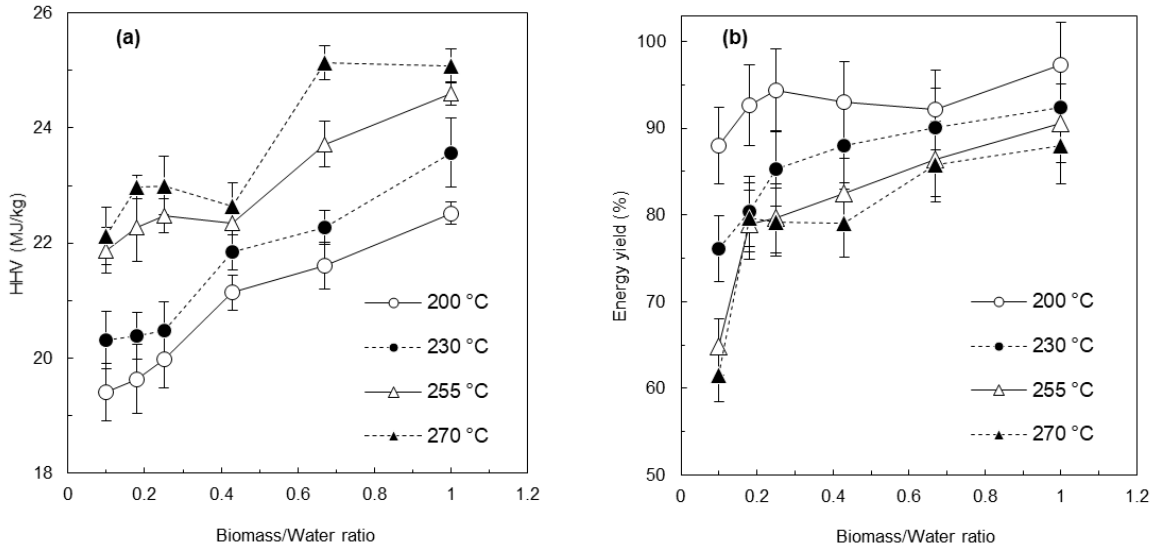

Figure 5: (a) Measured HHV and (b) EY at different B/W ratios and process temperatures.

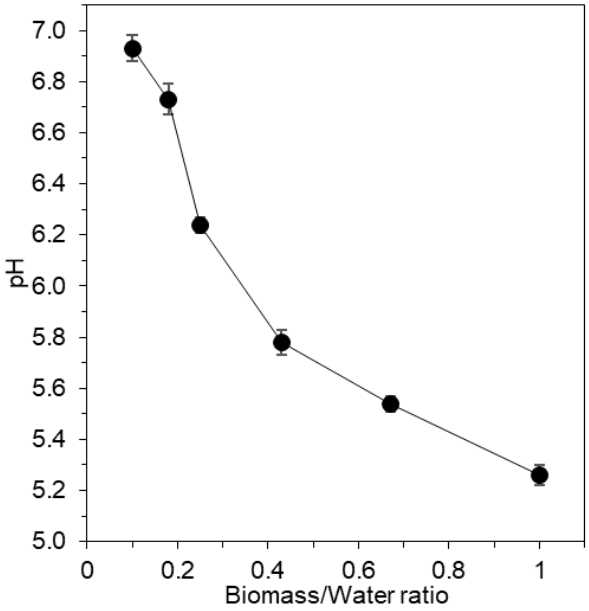

Figure 6: Effect of B/W ratio on the pH of the produced hydrochar

3.5 Proximate and ultimate analyses of the hydrochars.

The proximate and ultimate properties of the raw samples and produced hydrochars are presented in Table 1. Overall, the VM decreased and the FC and ash content increased with increasing temperature. For example, the VM decreased from 70.3% to 42.6% while the FC increased from 15.7% to 37.5% when the DM was hydrothermally treated at 270 °C at a B/W ratio of 1.0. The decreased VM may have been converted to other substances during the process, such as liquid or gaseous products, [66, 73] increasing FC. FR, which is the ratio of FC to VM and is used to rank fuel quality, [74] is thus increased by the process. The influence of the B/W ratio on the FR was more pronounced at higher B/W ratios across the process temperatures, indicating that higher quality hydrochars would be produced under V-HTC conditions. Indeed, the FR of the hydrochar at the predominantly V-HTC conditions of 270 °C and a B/W ratio of 0.67 to 1.0 was higher than 0.6 (reported for lignite) and close to 1.2 (reported for subbituminous

coal) [75, 76]. The ash content increased from 13.9% to 23.9% upon increasing the process temperature to 270 °C. Wu et al. [9] also observed an increased ash content of DM, from 24.2% to 40.4%, by increasing the process temperature to 280 °C, perhaps because ash in biomass increases upon further reduction in the VM at higher temperature. In contrast, the effect of the B/W ratio on ash content showed an unexpected trend. In general, the ash content of hydrochar can decrease in some cases because the ash may leach into the liquid phase during HTC [77]. Therefore, it was expected that the highest ash content would be observed at a B/W ratio of 1.0, since the higher the B/W ratio, the less likely such ash leaching would occur. However, the results showed an increasing trend in ash content up to B/W ratios of 0.43–0.67 and then a decrease in ash content at a B/W ratio of 1.0, where the liquid phase was the smallest. Perhaps vapor is more effective at leaching ash than bulk water, although we cannot currently offer a clear explanation.

Table 1. Proximate and ultimate analyses, and EDR of the hydrochars

Sample name		Proximate analysis (wt.%)			Ultimate analysis (wt.%)				FR (-)	EDR (-)
Temp. (°C)	B/W ratio	VM	*FC	Ash	C	H	N	O*		
Raw	-	70.3	15.7	13.9	42.6	5.4	1.9	36.2	0.223	-
200	0.1	63.3	21.6	15.1	47.9	5.2	2.2	29.6	0.341	1.13
	0.18	62.6	21.3	16.1	47.8	5.2	2.1	28.8	0.340	1.14
	0.25	62.1	20.8	17.2	47.8	5.2	2.1	27.7	0.335	1.16
	0.43	61.6	24.2	14.3	50.7	5.3	2.1	27.7	0.393	1.23
	0.67	58.7	24.8	16.6	48.7	5.2	2.1	27.5	0.422	1.26
	1.0	58.9	25.2	15.9	53.8	5.2	2.4	22.7	0.428	1.31
230	0.1	63.4	21.5	15.1	50.2	5.2	1.9	27.6	0.339	1.18
	0.18	59.6	24.5	15.8	50.5	5.2	2.1	26.4	0.411	1.19
	0.25	60.2	22.9	16.9	49.5	5.3	2.4	25.9	0.380	1.19
	0.43	55.2	23.6	21.1	53.8	5.1	2.4	17.6	0.428	1.27
	0.67	54.8	24.9	20.2	53.2	5.1	2.4	19.2	0.454	1.30
	1.0	54.4	28.3	17.4	53.8	5.2	2.4	22.7	0.520	1.37
255	0.1	50.8	26.1	23.1	55.4	5.1	2.4	14.1	0.514	1.27
	0.18	51.9	26.0	22.0	54.1	5.1	2.5	16.3	0.501	1.30
	0.25	51.1	29.5	19.4	55.7	5.2	2.6	17.1	0.577	1.31
	0.43	49.1	28.5	22.4	52.8	5.0	2.8	17.0	0.580	1.30
	0.67	47.4	28.4	24.3	56.7	4.9	2.6	11.6	0.599	1.38
	1.0	49.5	31.8	18.7	58.5	5.1	2.7	15.1	0.642	1.43
270	0.1	49.7	29.6	20.7	53.9	4.9	2.6	17.9	0.596	1.28
	0.18	48.1	30.0	21.9	53.8	4.9	2.7	16.6	0.624	1.33
	0.25	50.6	28.9	20.4	55.1	5.1	2.7	16.7	0.571	1.34
	0.43	45.2	30.9	23.9	53.9	4.8	2.9	14.4	0.684	1.31
	0.67	44.6	33.9	21.5	59.6	4.9	2.8	11.2	0.760	1.46
	1.0	42.6	37.5	19.9	59.1	5.0	2.8	13.3	0.880	1.46

*Calculated by difference

The ultimate analyses confirmed that the carbon content increased from 42.6% to 59.6% and the oxygen content decreased from 36.2 to 11.2% with increasing severity of the processing conditions. The change in hydrogen and nitrogen content was small: hydrogen decreased from 5.4% to 4.9% while nitrogen increased from 1.9% to 2.9%. Generally, oxygen in biomass is removed due to decarbonylation, decarboxylation and dehydration during the HTC process, and the degree of oxygen removal is pronounced at higher temperatures, increasing the relative carbon content of hydrochar [11,40–42]. This typical trend with increasing process temperature was observed in the present study.

Notably, the increase in carbon and the decrease in oxygen appeared to be promoted at higher B/W ratios. To understand the increase and decrease of carbon and oxygen in more detail, their percentage losses are shown in Figure 7. The use of a higher B/W ratio, which corresponds to the transition from L-HTC to V-HTC, tended to decrease carbon loss, showing that V-HTC is superior for retaining carbon in the hydrochar compared to L-HTC. This suggests that degraded substances deposited or chemically bonded to the hydrochar surface contain more carbon: i.e., more secondary char is formed in a V-HTC environment. The oxygen content of degraded substances is generally relatively high but oxygen is removed through dehydration or carboxylation before interaction with hydrochar, resulting in secondary char formation on hydrochar. More oxygen was removed with increasing B/W ratio at process temperatures of 200 °C and 230 °C but was little affected by the B/W ratio at higher temperatures of 255 °C and 270 °C. Thus, the impact of B/W ratio on deoxygenation is higher in mild HTC processes but the process temperature increases oxygen removal in severe HTC processes.

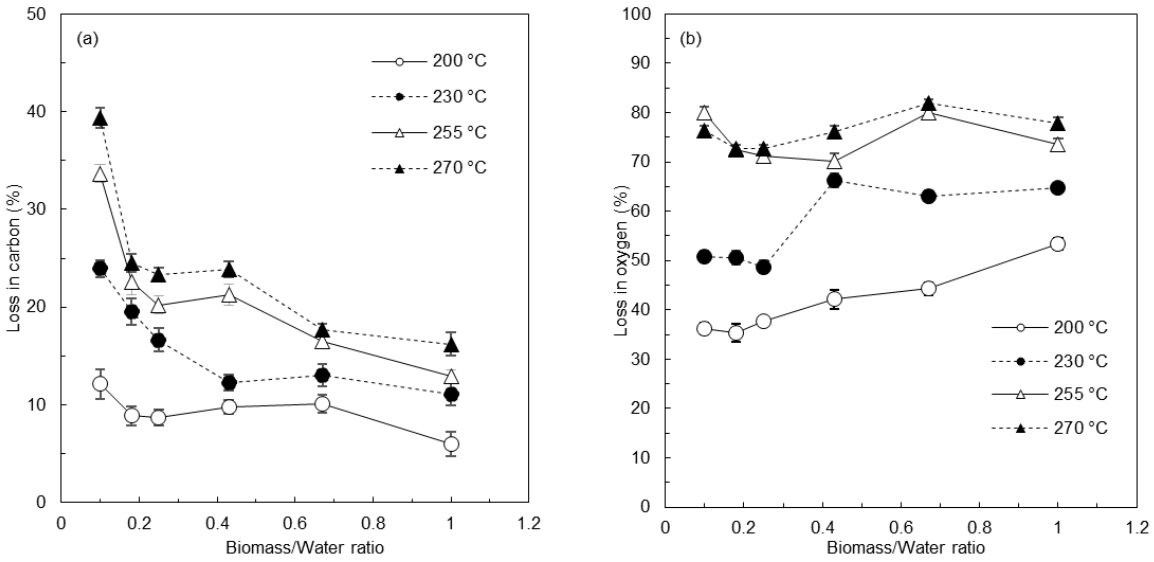

Figure 7: Losses in (a) carbon and (b) oxygen.

Data from the ultimate analyses were used to plot the van Krevelen diagram (Figure 8), which provides general information about the quality and type of fuel and alterations in biomass composition. A fuel with low atomic ratios of O/C and H/C is highly preferred because it produces less smoke, water vapor, and energy loss during combustion [17,33,43,44]. The diagram showed that the degree of coalification of the hydrochars increased as the temperature and B/W ratio increased. Thus, increasing the B/W ratio from 0.1 to 1.0 at each temperature is effective for decreasing the O/C and H/C ratios of the raw feedstock. At a given temperature, the use of a higher B/W ratio gave lower atomic ratios of O/C and H/C, showing that a higher quality solid biofuel can be produced through predominantly V-HTC conditions rather than L-HTC. For example, hydrochars produced at between 200 °C at a B/W ratio of 0.1 up to 230 °C at a B/W ratio of 0.43 were peat-like, hydrochars produced at 230 °C at a B/W ratio of 0.67 up to 270 °C at a B/W ratio of 0.43 were lignite-like, and hydrochars produced at 255 °C at a B/W ratio of 0.43 and at 270 °C at B/W ratios of 0.67 and 1.0 were coal-like.

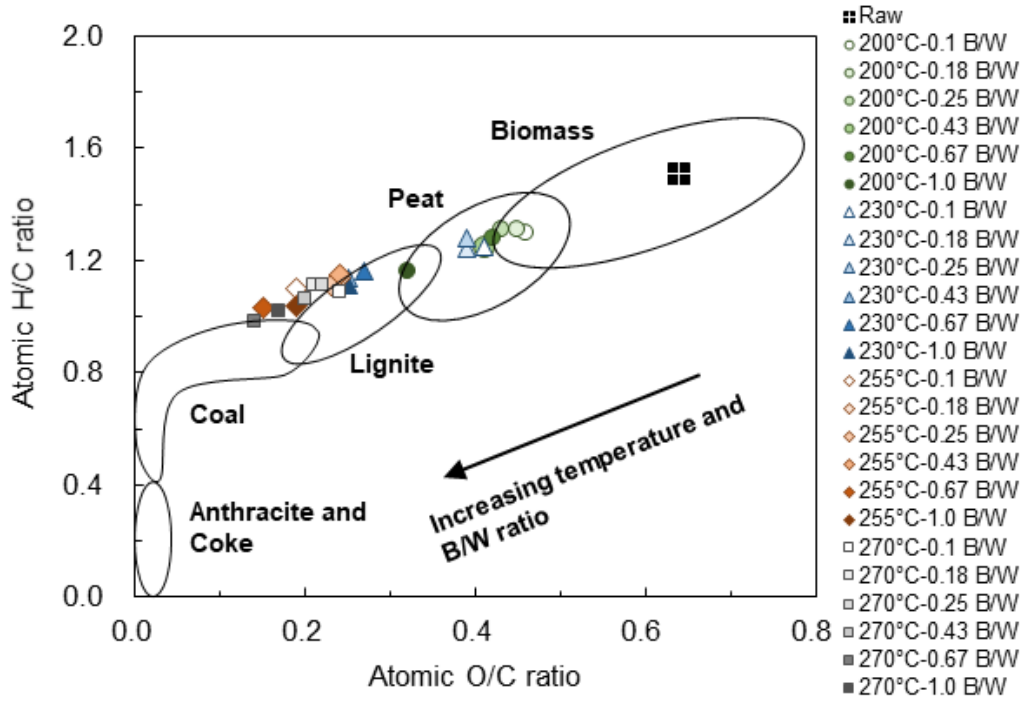

Figure 8: van Krevelen diagram for the hydrochars

3.6 Thermal behaviour and combustion parameters

Figure 9 shows the TG and the DTG curves for the hydrochars produced at 270 °C using a heating rate of 10 °C/min. As shown in Figure 7b, regardless of the B/W ratio, four distinctive peaks were observed corresponding to the loss of moisture (50 to 200 °C), low molecular weight volatiles (200 to 300 °C), lignin decomposition (300 to 400 °C), and char combustion (450 to 600 °C) [6, 75]. The decomposition peaks tended to decrease with increasing B/W ratio and the smallest peak was observed at 270 °C and a B/W ratio of 1.0, probably due to this hydrochar having the lowest VM and highest FC (Table 1). Progressive reduction in the decomposition peaks at higher B/W ratios indicates enhanced thermal stability of the hydrochar [81].

The ignition temperature (T_i) is an important combustion parameter to determine the probability of fire or explosion when using a hydrochar as a solid biofuel [44,45]. The

hydrochar produced at 270 °C and a B/W ratio of 0.1 has the lowest T_i while the hydrochar produced at 270 °C and a B/W ratio of 1.0 has the highest T_i, as shown in Table 2. The increase in T_i is due to reduction of the VM content in the hydrochar during the process [81]. Thus, the safety of hydrochars during handling, storage and transportation as solid biofuels increases as the B/W ratio is increased [37,46]. On the other hand, the CCI and CSI decreased with increasing B/W ratio, suggesting that the combustibility of hydrochars produced under V-HTC is lower than those produced under L-HTC. However, excessive VM increases the CCI and CSI, may cause an unstable flame and combustion and leading to high heat loss [74]. Thus, combustion performance of the prepared hydrochars should be explored in more detail in future studies.

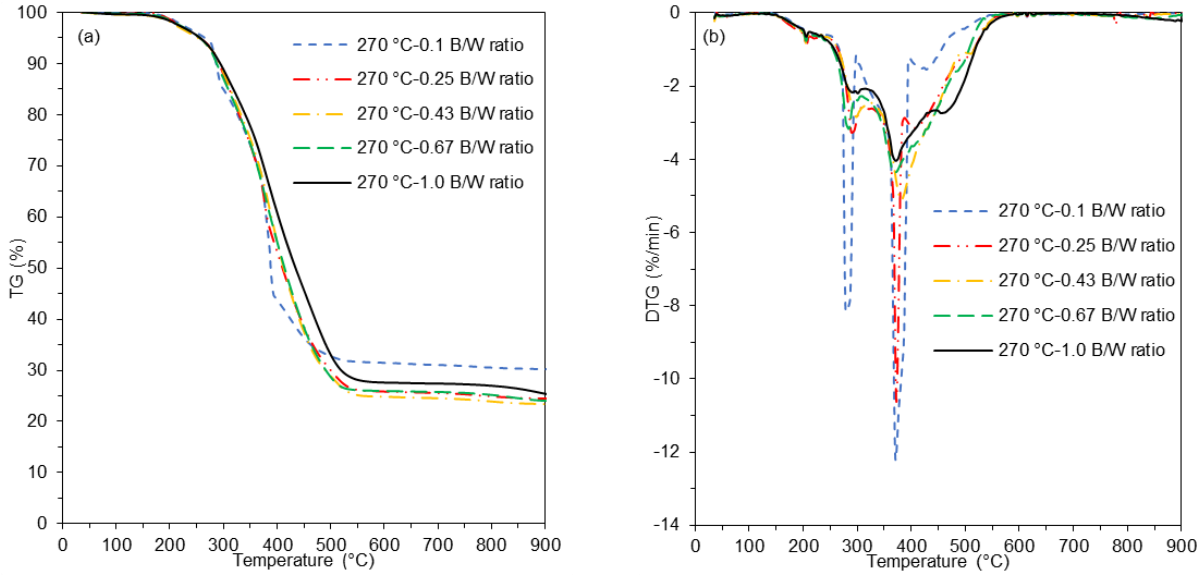

Figure 9: (a) TG for hydrochars at 270 °C (b) DTG for hydrochars at 270 °C

Table 2. Combustion parameters determined from the TGA curve at 10 °C/min (270 °C)

Sample	T_i (°C)	T_m (°C)	DTG_m (%/min)	DTG_{av} (%/min)	T_b (°C)	B_t (min)	R_m (%)	*CCI* ($min^{-2} \times °C^{-3}$)	*CSI* ($min^{-1} \times °C^{-2}$)
0.1 B/W	218.8	354.7	-12.1	-0.8	511.7	50	29.6	3.9×10^{-7}	1.3×10^{4}
0.25 B/W	223.5	371.8	-10.6	-0.9	555.5	51	24.4	3.4×10^{-7}	1.1×10^{4}
0.43 B/W	223.4	380.7	-5.1	-0.9	563.9	52	23.3	1.6×10^{-7}	5.2×10^{3}
0.67 B/W	223.5	372.5	-4.3	-0.9	564.2	52	24.0	1.4×10^{-7}	4.4×10^{3}
1.0 B/W	223.8	374.7	-3.9	-0.9	573.3	54	25.3	1.2×10^{-7}	3.9×10^{3}

T_i: ignition temperature; T_m: peak temperature; DTG_m: the maximum mass loss rate; DTG_{av}: average mass loss rate; T_b: burn out temperature; B_t: burn out time; R_m: residual mass; *CCI*: comprehensive combustion index; *CSI*: combustion stability index

CONCLUSION

This study investigated the hypothesis that hydrochar with improved fuel properties would be produced from low moisture content biomass without the need to add water. To verify the hypothesis, DM at high and low moisture conditions was hydrothermally treated using L-HTC and V-HTC conditions. The results showed that the V-HTC process is superior to the L-HTC process in improving the fuel properties of DM. The V-HTC process is conducted at a higher B/W ratio, where the lower liquid content may facilitate the formation of secondary char on the hydrochar surface and increase the severity of the reaction due to the higher acid content, resulting in higher energy densification and mass yield. As a result, the V-HTC process is expected to have a higher hydrochar production capacity and require less water compared to the L-HTC process. Proximate analysis revealed that the ash content was the maximum at B/W ratios of 0.43 and 0.67 rather than 1.0, and thus further studies are required to understand this behaviour. The obtained results nonetheless support the hypothesis of the study.

Declaration of Competing Interest

The authors declare that they have no known competing financial interests or personal relationships that could have appeared to influence the work reported in this paper.

ACKNOWLEDGEMENTS

The authors acknowledge the Instrumental Analyses Division of Hokkaido University, Japan, for performing elemental analyses of the samples. The authors also acknowledge the Centre for Advanced Research of Energy and Materials, Faculty of Engineering, Hokkaido University, Japan, for granting permission to the authors to perform thermal analyses in its laboratory.

CHAPTER 4

Upgrading the fuel properties of hydrochar by co-hydrothermal carbonization of dairy manure and Japanese larch (*Larix kaempferi*): product characterization, thermal behaviour, kinetics, and thermodynamic properties

Mohammed Aliyu[1,2], Kazunori Iwabuchi[3], Takanori Itoh[4]

[1]Graduate School of Agriculture, Hokkaido University, Kita 9, Nishi 9, Kita-ku, Sapporo, Hokkaido 060-8589, Japan

[2]Agricultural and Bioresources Engineering, Federal University of Technology, P. M. B. 65, Minna, Niger State, Nigeria

[3]Research Faculty of Agriculture, Hokkaido University, Kita 9, Nishi 9, Kita-ku, Sapporo, Hokkaido 060-8589, Japan

[4]Tanigurogumi Corporation, Shiobara 1100, Nasushiobara, Tochigi 329-2921, Japan

[*]Corresponding email: iwabuchi@bpe.agr.hokudai.ac.jp

Graphical abstract

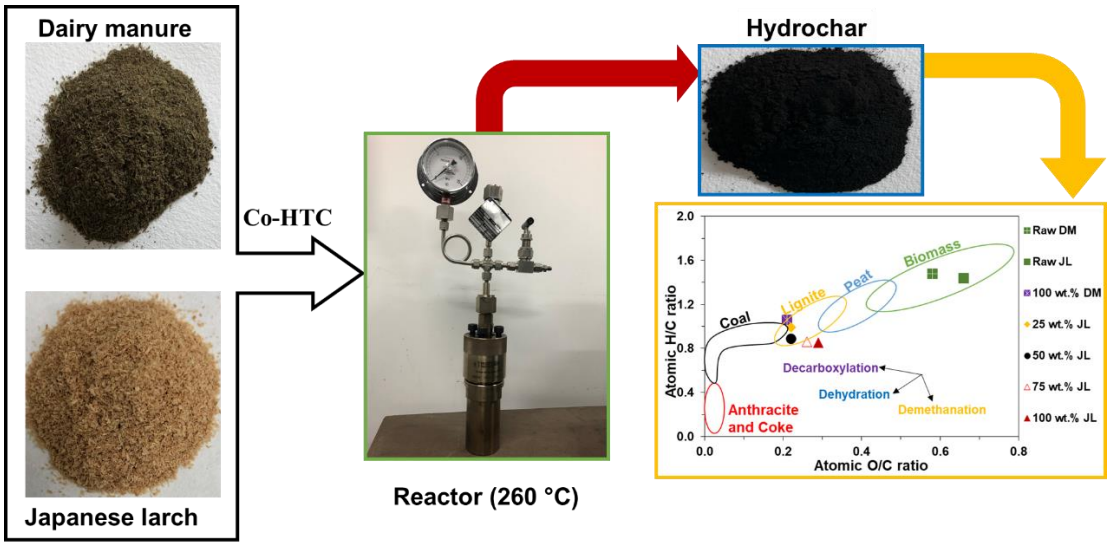

Abstract

This study investigated co-hydrothermal carbonization (co-HTC) of dairy manure (DM) and wood shavings from *Larix kaempferi*, commonly known as the Japanese larch (JL) to enhance the fuel properties of the resulting hydrochar. The JL was mixed with the DM at 25, 50 and 75 wt.% ratios. Co-HTC was conducted at 260 °C for 20 minutes. The resulting hydrochars were characterised based on the physicochemical properties and the thermal behaviour. Results showed that the hydrochar solid biofuel properties improved as the ratio of JL was increased. The produced hydrochars were in the region of lignite and closed to the region of the coal with increased fixed carbon, carbon contents and lowered H/C and O/C ratios. Hydrochar with ash content of 7.2±0.5% was obtained at 75 wt.% JL. In addition, the higher heating value (HHV) of hydrochar increased remarkably to 26.4±0.02 MJ/kg as the mass ratio of the JL was increased. The surface morphology of the hydrochars were altered and became distinct while the specific surface area (SSA) and the total pore volume (TPV) of the hydrochars increased at increasing the mass ratio of the JL. The surface functional groups were also altered by the co-HTC process. A decline in the combustion performance was observed after the HTC process but improved at 75 wt.% JL after the co-HTC process. The kinetic analysis also revealed that the activation energy decreased after the HTC process but increased to a higher value at 50 wt.% JL after the co-HTC process. Therefore, hydrochar production by co-HTC of DM and JL has proved to be an effective and promising solid biofuel source.

Key words: Japanese larch, Dairy manure, Thermochemical conversion, Co-hydrothermal carbonization, Hydrochar, Solid biofuel

1 Introduction

The fast depletion of fossil fuel reserves across the world and subsequent environmental pollution such as the green house gas emission has made biomass an attractive source of energy [4, 5]. Waste biomass such as animal manure is increasingly gaining attention due to the fast-growing animal husbandry across the world [6]. For this reason, animal manure generation have been reported in billions of tons in some countries annually [6, 7]. In Hokkaido prefecture of Japan alone, about 20 million tons of animal manure is generated annually [8]. Hence, biomass from animal manure could become one of the sustainable sources of biofuel production [6, 9]. However, there are limitations to the use of animal manure as a combustion feedstock due to its high moisture content, high ash content, poor grindability, and low energy density which can result in low combustion efficiency [6, 11]. To overcome some of these aforementioned drawbacks, it is necessary to pretreat animal manure to improve its fuel property. One of the pretreatment techniques that is used to upgrade the fuel property of animal manure is hydrothermal carbonization (HTC) [6, 9, 56].

HTC is an effective technique to carbonize and improve the fuel property of animal manure as a solid biofuel source [6, 9]. The conversion process uses hot compressed fluid at a moderate temperature range of 180 to 260 °C in an autoclave reactor [5, 11]. Unlike other available thermal conversion technologies for biomass, HTC does not need the pre-drying of a feedstock before carbonization [5] and therefore, appropriate to convert high moisture content animal manure to solid biofuel. However, animal manure is recognised as a high ash content feedstock after HTC pre-treatment [7, 9, 27, 28]. For instance, Wu *et al*. [9] and Gao *et al*. [27] reported ash contents of 39.48 wt.% and 40.66 wt.% with higher heating values (HHV) of 17.86 and 19.88 MJ/kg in hydrochar after HTC treatment

of dairy manure (DM) at 260 °C. Reza *et al*. [28] also reported an ash content of 25.36 wt.% and a HHV of 22.1 MJ/kg after the HTC pre-treatment of cow manure at 260 °C. These high ash contents of the carbonized solid biofuel from animal manure mentioned above could result in severe ash related problems such as fouling and scaling deposits if directly used for combustion. Consequently, this can lead to a reduction in the available area for heat transfer in a furnace and some connecting sections of combustion equipment [30]. It is, therefore, imperative to consider a technique that could further help to improve the fuel property and reduce the ash content in animal manure for efficient utilization as a solid biofuel.

Co-hydrothermal carbonization (co-HTC) of animal manure and a lignocellulosic biomass is a promising technique for the production of hydrochar with high energy recovery and low ash content [6]. In co-HTC, two or more feedstocks with distinct properties are mixed and carbonized to improve the fuel properties of the composite [84–87]. At present, several studies have reported a co-HTC of lignocellulosic biomass with other feedstocks such as coal, sewage sludge, medical waste, iron sludge, food waste and polyvinyl chloride [88]. However, limited study is available on the co-HTC of animal manure and lignocellulosic biomass. To the authors knowledge, only a co-HTC of swine manure and lignocellulosic biomass have been reported to date [6, 89]. Owing to the heterogeneous and different biochemical properties of animal manure, co-HTC of DM and wood shavings from *Larix kaempferi*, commonly known as the Japanese larch (JL), would provide additional insight into the synergistic effect of the co-HTC process on the resulting solid biofuel. The JL is a potential biofuel source that is generated as wood shavings during wood processing, and it is recognised as a low ash content lignocellulosic biomass thus may result in a positive synergistic effect with the DM [90].

Synergistic effect in co-HTC refers to the consequences of the interaction between the composite raw feedstocks which can result in a positive or a negative effect. If the total value of observed property after the co-HTC process is more than the total values for the individual feedstocks, it is considered a positive synergistic effect while the opposite is considered a negative effect [88]. Hence, the co-HTC of these two distinct biomasses may produce hydrochar of notable quality and affect the structural and functional groups inherent in the individual hydrochars. Also, the data obtained could provide some useful insights during the design of combustion equipment.

To design a combustion equipment at an industrial scale, it is necessary to understand the combustion behaviour, kinetics, and thermodynamic properties of a solid biofuel. To achieve this, isoconversional model-free kinetics is sometimes employed by using the data generated from thermogravimetric analysis (TGA) [3, 19]. Isoconversional model-free kinetics such as the Flynn-Wall-Ozawa (FWO) and Kissinger-Akahira-Sunose (KAS) are useful methods for determining the kinetic parameters of biomass decomposition, based on the data obtained from TGA [49, 91]. However, no available published data on the combustion behaviour, kinetic and thermodynamic properties of hydrochar from the co-HTC of DM and JL at varying mass ratios have been reported. Hence, the objective of this study was to investigate the changes in the fuel properties, structural morphology, functional group, and combustion characteristics of hydrochar from the co-HTC of JL and DM.

2 Materials and methods

2.1 Materials

DM was obtained from an experimental farm of Field Science Centre for Northern Biosphere, Hokkaido University, Japan. For experimental purposes, the DM sample was dried in an electric oven for 24 hours at 105 °C to a constant mass. The JL wood shavings were obtained from the wood engineering laboratory of Hokkaido University, Japan, and was also dried to a constant mass. The dried samples were milled using a portable electric milling machine to ensure thorough mixing in ratios. The JL wood shavings were mixed in mass ratios with the DM at 25, 50 and 75 wt.%. The prepared samples were sealed in plastic bags and stored before the co-HTC experiment (appendix B).

2.2 HTC reactor set-up and procedure

Co-HTC experiments were performed in a 70 mL stainless steel batch reactor TVS-N2 (Taiatsu Techno, Tokyo, Japan) with a temperature and pressure limits of 300 °C and 8 MPa. For each batch of the experiment, 10±0.01 g of oven-dried sample and 10±0.01 g distilled water (B/W ratio = 1.0) were well mixed and placed in the reactor. The reactor was sealed, oxygen was swept out from the sealed reactor by flushing with pure nitrogen gas thrice. The reactor's temperature was controlled by a PID (proportional-integral-derivative) to the desired HTC temperature. A reaction temperature of 260 °C was used while reaction time at peak temperature was kept for 20 minutes for all the experiments. A reaction temperature of 260 °C was chosen because it is considered an appropriate temperature to produce hydrochar of a coal-like properties [5]. Holding time of 20 minutes at peak temperature was used to minimize a further mass loss [13, 36, 92].

After terminating the reaction, the reactor was placed in cold water for rapid cooling. The pressure release valve was opened, and the gaseous products were vented into a fume hood. The solid hydrochar was recovered from the reactor and weighed. The recovered hydrochar was dried in an electric oven at 105 °C for 24 hours. The dried hydrochar was milled, sieved, and stored in sample bottles for analyses. The produced hydrochars were named 100 wt.% DM, 25 wt.% JL, 50 wt.% JL, 75 wt.% JL and 100 wt.% JL. Each batch of the experiment was conducted thrice with the respective means recorded with standard deviations.

2.3 Properties and analytical determination

The mass yield of hydrochar (MY), the energy densification ratio (EDR), and the energy yield (EY) were calculated using Eqs (1) to (3) [84, 93]. The calorific values were determined using an OSK 200 bomb calorimeter (Ogawa Sampling, Saitama, Japan) by combusting at least 0.5 g of each sample in a calorimeter with oxygen at 0.3 MPa [67].

$$MY\ (\%) = \frac{m_{\mathrm{hc}}}{m_{\mathrm{f}}} \times 100 \quad (1)$$

$$EDR = \frac{HHV_{\mathrm{hc}}}{HHV_{\mathrm{f}}} \quad (2)$$

$$EY\ (\%) = \left[MY \times \left(\frac{HHV_{hc}}{HHV_{\mathrm{f}}}\right)\right] \times 100 \quad (3)$$

where m_{hc} (g) is the dry mass of the hydrochar, m_{f} (g) is the dry mass of the raw feedstock, and HHV_{hc} (MJ/kg) and HHV_{f} (MJ/kg) are the higher heating values of the hydrochar and raw feedstock.

The ash contents of the samples were determined using an electric muffle furnace (ADVANTEC, FUL220FA, Japan) by incinerating 1 g at 600 °C for 3 hours. The volatile matter (VM) was determined using ASTM standard procedure (E872) by heating the

samples at 950 °C for 7 minutes in an electric furnace. Then, the fixed carbon (FC [%] = 100 − VM [%] − ash [%]) and the fuel ratio (FR = FC/VM) were calculated.

The carbon, hydrogen, and nitrogen (C, H and N) contents in the samples were determined using an elemental analyser (Exeter Analytical, North Chelmsford, MA, USA) and the oxygen content was calculated by difference (O [%] = 100 − C [%] − H [%] − N [%] − ash [%]). The carbon retention (CR) was calculated using Eq (4).

$$CR\ (\%) = \left(\frac{C_{\mathrm{hc}}}{C_{\mathrm{f}}}\right) \times MY \qquad (4)$$

where C_{hc} and C_{f} are the wt.% of carbon in hydrochar and the raw sample, respectively. Note that C_{f} is also the wt.% of carbon in the raw mixtures. The raw mixtures were thoroughly mixed in mass ratios, milled and the ultimate compositions were determined using an elemental analyser as well.

The surface morphology of the raw samples and the hydrochars were captured using an SEM (Scanning Electron Microscopy) analyser (JEOL JSM-7001FA, USA) at 15 kV and a working distance of 10 mm. Furthermore, to elucidate the changes in the surface characteristics and for potential usage in soil amendment and adsorption of contaminants in aqueous solutions, the Brunauer-Emmett-Teller (BET) specific surface area (SSA), total pore volume (TPV) and average pore diameter (APD) were determined by BelsorpII mini. The Fourier transform infrared spectroscopy (FTIR) was performed using JASCO IRT-3000 N spectrometer with attenuated total reference (ATR) accessory. FTIR spectra from 128 scan were recorded in the wavenumber range of 4000 to 500 cm^{-1} with a 4 cm^{-1} resolution.

2.4 Thermal analysis

To observe the combustion behaviour of the hydrochars at different heating rates, a combustion experiment was performed in a thermal analyser (TGA/DSC 3^+, METTLER TOLEDO, USA) under an air atmosphere. To eliminate heat and mass transfer limitation within the sample, about 25 mg of sample was placed in a 150 μL aluminium oxide (Al_2O_3) crucible. The sample was heated from the room temperature to 900 °C with an airflow rate of 100 mL/min at the heating rates of 5, 10, 15 and 20 °C/min. For each sample, the TGA experiment was repeated at least twice for accuracy. The thermogravimetric (TG) and differential thermogravimetric (DTG) data were used to determine some characteristic temperatures and combustion parameters which include the ignition temperature (I_T), the burnout temperature (B_T), the temperature at maximum decomposition (T_m), the burn out time (B_t), the residual mass (R_m), the maximum mass loss rate (DTG_{max}) and the average mass loss rate (DTG_{av}). The I_T (°C) indicates the temperature at which the fuel starts to burn while B_T (°C) denotes the temperature for the complete combustion of the fuel and were determined by the TG-DTG tangent method [6, 48]. The T_m (°C) is the temperature at the maximum mass loss rate (DTG) or the peak temperature. The R_m (%) is the percentage of the residue left after complete combustion of the sample. Furthermore, to evaluate the combustion performance of the raw samples and the hydrochars, the comprehensive combustion index (CCI) and combustion stability index (CSI) were calculated using Eqs (5) and (6), respectively [6, 47, 69, 94].

$$CCI = \frac{DTG_{max} \times DTG_{av}}{I_T^2 \times B_T} \quad (5)$$

$$CSI = 8.5875 \times 10^7 \times \frac{DTG_{max}}{I_T \times T_m} \quad (6)$$

2.4.1 Kinetics and thermodynamic properties of activation

To determine the activation energy through TGA, more than one heating rate is required to plot a regression line [6, 49]. The heating rates of 5, 10, 15 and 20 °C/min were used to study the combustion kinetics of the raw samples and the hydrochars using non-isothermal isoconversional model-free methods. These methods were applied to convert the mass loss data obtained by TGA analysis into the conversion rate (α) as shown in Eq (7), while the activation energies were calculated using the Flynn-Wall-Ozawa (FWO) and Kissinger-Akahira-Sunose (KAS) methods using Eqs (8) and (9), respectively. The thermodynamic properties namely, the pre-exponential factor (A), Gibbs free activation energy ($\Delta G^{\ddagger}$), enthalpy of activation ($\Delta H^{\ddagger}$), and the entropy of activation ($\Delta S^{\ddagger}$) were determined using Eqs (10) to (13) [2, 6].

$$\alpha = \frac{m_0 - m}{m_0 - m_f} \tag{7}$$

$$\ln \beta = ln \frac{AE_a}{RG(\alpha)} - 5.331 - 1.052 \frac{E_a}{RT} \tag{8}$$

$$\ln\left(\frac{\beta}{T^2}\right) = \ln\left(\frac{AR}{E_a G(\alpha)}\right) - \frac{E_a}{RT} \tag{9}$$

$$A = \frac{\beta\, E_a\, e^{\frac{E_a}{R\,T_m}}}{R\, T_m^2} \tag{10}$$

$$\Delta G^{\ddagger} = E_a + R\ T_m \ln\left(\frac{k_B\, T_m}{h\, A}\right) \tag{11}$$

$$\Delta H^{\ddagger} = E_a - RT_m \tag{12}$$

$$\Delta S^{\ddagger} = \frac{\Delta H^{\ddagger} - \Delta G^{\ddagger}}{T_m} \tag{13}$$

Here, α is the conversion rate, m_0 is the initial mass (mg), m is the actual mass, m_f is the final mass, A (s^{-1}) is a pre-exponential factor, R is the universal gas constant 8.314 J K^{-1} mol^{-1}, $G(\alpha)$ is the mechanism function and T is the absolute temperature (K) and T_m is the temperature at maximum mass loss rate, h is the Planck's constant (6.63×10^{-34} m^2 kg s^{-1}), k_B is the Boltzmann constant (6.63×10^{-23} m^2 kg s^{-2}), $\ln \beta$ or $\ln\left(\frac{\beta}{T^2}\right)$ versus 1/T was plotted as a straight line at the different heating rates (β) of 5, 10, 15 and 20 °C/min. The activation energies (E_a) were calculated for each α from the slope of the regression lines of $\ln \beta$ versus 1/T for FWO and $\ln\left(\frac{\beta}{T^2}\right)$ versus 1/T for KAS.

3 Results and discussion

3.1 Hydrochar yield

The MY of hydrochars at the different mixed ratios is shown in Table 1. The MY slightly decreases with increasing proportion of the JL. The highest MY of 61.5±2.5% was observed at 25 wt.% JL. The decreasing MY as a result of increasing wt.% of the JL could be attributed to the decreasing ash content (Table 1). Ash is reported to be an inert material that does not participate in HTC reactions, hence decreasing ash content of the co-HTC process may have contributed to the decreasing MY [84]. A similar observation was reported by He *et al*. [84] where the increasing proportion of rice straw ratio to sewage sludge decreases the MY of hydrochar and was attributed to the decreasing ash content.

3.2 Proximate and ultimate properties of the hydrochars

The proximate and the ultimate properties of the raw samples and the hydrochars are presented in Table 1. The VM of the hydrochars were significantly lowered after the conversion process. The results indicated that the VM may have been converted to other

substances during the process, such as liquid or gaseous products [34]. The FC is one of the quality indices of a solid biofuel. The FC for the hydrochar 100 wt.% DM was 30.1±0.9% and increased remarkably to 47.3±0.6% after co-HTC with the JL. The increased FC at increasing wt.% of JL is likely due to the decreasing ash content for the co-HTC process. The FC for the 100 wt.% JL and 75 wt.% JL became almost equal in value after the co-HTC process. This indicates that the co-HTC of DM and JL is an effective technique to produce hydrochar with improved fuel properties. He *et al*. [84] and Zhang *et al*. [93] reported similar observations for the co-HTC of sewage sludge/rice straw and corn stalk/swine manure, respectively. The ash content of the hydrochar decreased as the wt.% of the JL was increased due to the lower ash property of the JL. The ash content of 100 wt.% DM hydrochar was 25.9±0.8% but after co-HTC, hydrochar of a lower ash content of 7.2±0.5% was obtained at 75 wt.% JL. The difference in the ash content of 75 wt.% JL and 100 wt.% DM amounts to 72.1%, suggesting that the JL is an effective feedstock to improve the fuel properties of a high ash feedstock such as the DM. This could reduce ash related problems such as fouling and slagging if used in a combustion equipment. A similar observation was also reported by Lang *et al*. [89] where the increase in the proportion of cornstalk ratio to swine manure produced hydrochar with an ash content of 8.17±0.25%.

The FR can be used to rank hydrochar as a coal-like solid fuel [74]. The FR of the hydrochars is shown in Table 1. After co-HTC, FR of the hydrochars increased as the blending ratio of the JL in the mixture was increased. The observed increase could be attributed to the increasing FC, relative to the VM. The highest FR of 1.0±0.01 observed at 75 wt.% JL showed that the increased wt.% of the JL has improved the fuel property of the hydrochar after the co-HTC process and hence a positive synergy. It was also

observed that the FR of the hydrochars were higher than 0.6 reported for lignite and very close to 1.2 reported for a sub-bituminous coal [76, 84].

The carbon content of the hydrochars increased after the HTC and co-HTC pre-treatments. The observed increase in the carbon content was due to the dehydration and decarboxylation reactions during the conversion process [15]. Furthermore, increasing the proportion of JL significantly increases the carbon content of the hydrochars. The increased carbon content could be related to the higher carbon content of the JL which may have augmented the carbon content of the hydrochars from the co-HTC process. Hence, the carbon content improved to 65.0±0.2% at 75 wt.% JL after the co-HTC process. The hydrogen content of the hydrochars decreased compared to the raw feedstocks likely due to dehydration reaction during conversion [5]. However, the hydrogen content of the hydrochars remained almost the same at increasing wt.% of the JL possibly owing to the use of the same reaction severity (same production temperature of 260 °C). The nitrogen content of the 100 wt.% DM increased from 2.1 to 2.9%, this is consistent with the study by Reza *et al*. [28] where the increased nitrogen content in hydrochar from cow manure after HTC pre-treatment at 260 °C was attributed to the adsorption of degraded nitrogen from protein in cow manure at higher HTC temperature. Thereafter, the nitrogen content decreased from 2.9% to 0.84% as the proportion of JL was increased. This could be attributed to the lower nitrogen content of the JL with a higher proportion of JL lowering the nitrogen content of the hydrochars from the co-HTC process. Decreased oxygen content was observed in the hydrochars at the different blend ratios after the conversion of the raw samples. The removal of oxygen from the raw samples is very important to increase the energy density [9]. The removal of oxygen was due to dehydration and decarboxylation reactions during the conversion process [27, 78,

79]. However, the oxygen content of the hydrochars increases as the wt.% of JL was increased. This could be attributed to the higher oxygen content in the raw JL (Table 1) which may have contributed to the increased oxygen contents of the hydrochars from the co-HTC process. The results of the calculated carbon retention are presented in Table 1. The CR was enhanced to 84.5±3.4 at 75 wt.% JL. This showed that the co-HTC treatment of JL and DM was an effective for carbon retention in a solid biofuel.

3.3 HHV, energy densification ratio and energy yield of the hydrochars

The HHV of the hydrochars increases remarkably as the ratio of the JL was increased (Table 1). The co-HTC process enhanced the HHV to 26.4±0.02 MJ/kg. This enhancement in the HHV was not surprising, considering the initial higher HHV of the JL. The improvement in the HHV of the hydrochars after co-HTC may have been partly contributed by the higher carbon and lower ash contents of the JL. The improved HHV reported in this study suggested that the co-HTC of DM and JL was effective in upgrading the energy property of hydrochar as a solid biofuel. He *et al*. [84], Wang *et al*. [95] and Ma *et al*. [96] reported a similar trend for sewage sludge/rice straw, food waste/woody biomass, and sewage sludge/sawdust co-HTC, respectively. The EDR was calculated to evaluate the degree of energy densification after the conversion process. Expectedly, the EDR showed a similar trend to that of the HHV, with a maximum EDR of 1.44 observed at 75 wt.% JL after the co-HTC process. The EY also slightly increased progressively as the mass ratio of the JL was increased. The EY improved to 84.9±0.02% (Table 1). The EY was not expected to change significantly because it is dependent on the MY which did not change significantly as well.

Table 1 Mass yield, proximate, ultimate, (wt.%) and energy properties of the hydrochars at 260 °C

Parameters	Raw DM	Raw JL	100 wt.% DM	25 wt.% JL	50 wt.% JL	75 wt.% JL	100 wt.% JL
MY (%)	-	-	59.7±3.4	61.5±2.5	59.2±1.5	58.9±3.9	59.1±2.8
Proximate properties							
VM (%)	65.1±0.3	85.8±0.3	43.9±0.5	46.1±0.5	44.5±0.1	45.5±0.1	51.8±0.6
FC* (%)	15.9±0.6	14.2±0.3	30.1±0.9	32.4±0.4	42.5±0.3	47.3±0.6	47.6±0.2
Ash (%)	18.9±0.4	0.08±0.1	25.9±0.8	21.5±0.6	13.0±0.6	7.2±0.5	0.59±0.5
FR	0.25±0.01	0.29±0.01	0.68±0.03	0.70±0.01	0.95±0.1	1.0±0.01	0.92±0.01
Ultimate properties							
C (%)	41.6±0.3	49.7±0.1	51.9±0.1	55.3±0.4	62.3±0.3	65.0±0.2	67.9±0.3
H (%)	5.1±0.04	5.9±0.07	4.6±0.02	4.6±0.04	4.7±0.01	4.7±0.04	4.8±0.03
N (%)	2.1±0.00	0.3±0.1	2.9±0.00	2.3±0.00	1.6±0.00	0.84±0.00	0.30±0.00
O* (%)	32.3±0.3	44.0±0.1	14.7±0.1	16.4±0.4	18.4±0.3	22.3±0.2	26.4±0.3
CR (%)	-	-	73.9±4.8	74.3±6.9	83.0±1.8	84.5±3.4	81.7±3.3
Energy properties							
HHV (MJ/kg)	16.9±0.03	18.8±1.5	21.9±0.08	22.9±0.05	25.1±0.02	26.4±0.02	27.4±0.1
EDR	-	-	1.29±0.01	1.31±0.03	1.40±0.08	1.44±0.12	1.45±0.12
EY (%)	-	-	77.4±0.08	80.8±0.05	82.9±0.02	84.9±0.02	85.9±0.1

*Calculated by difference

3.4 van Krevelen diagram for the raw samples and the hydrochars

To elucidate the changes in the atomic ratios of the raw biomass and the hydrochars, data from elemental analyses was used to plot the van Krevelen diagram. The van Krevelen diagram can provide some insight into the type and quality of fuel and the reflection in the alteration of biomass composition. A fuel with a lower O/C and H/C atomic ratio is highly preferred due to its decreased smoke, water vapour and energy losses experienced during combustion [71, 80, 97]. To explain the changes in the atomic ratio composition

of raw samples and the produced hydrochars, the atomic ratios of H/C and O/C were calculated and plotted in a van Krevelen diagram using the data from elemental analysis (Fig. 1). In this diagram, the atomic ratios of H/C and O/C moved from the top right to the bottom left-hand corner after the conversion process. The decreased H/C and O/C ratios suggested increased aromatization or coalification degree, which can be beneficial for carbon sequestration [93, 98]. Fig. 1 showed that aromatization or coalification degree of the produced hydrochars from the co-HTC process was enhanced. A similar observation was reported for sewage sludge and pinewood sawdust from co-HTC by Zhang *et al*. [93]. The hydrochars fell within the region of lignite and closed to the coal region. Therefore, the hydrochars can be used for pulverised coal injection in a furnace for co-combustion with coal since they matched some atomic ratios close to those of a coal [99].

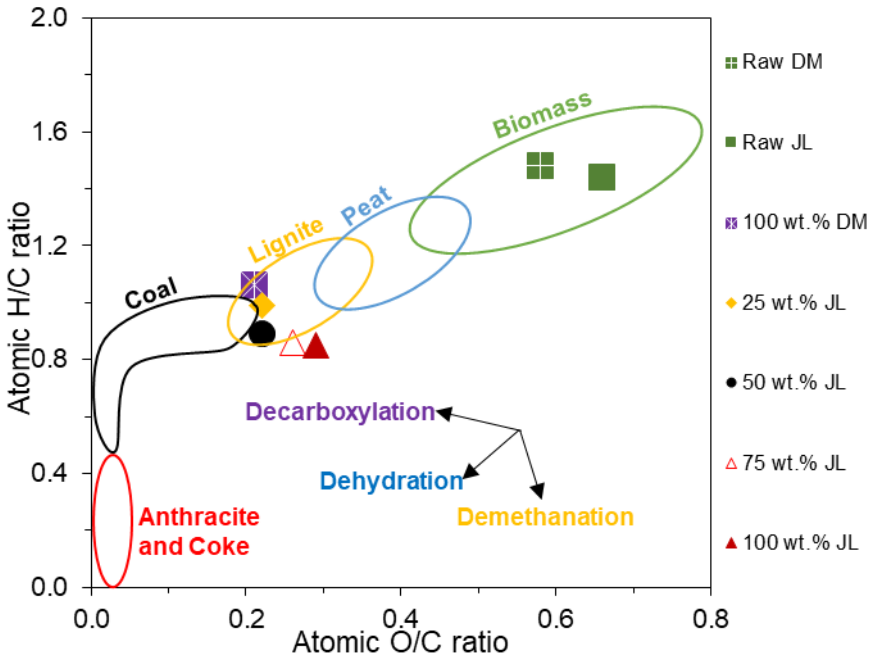

Fig. 1 the van Krevelen diagram for the raw samples and the hydrochars

3.5 Surface morphology of the raw and hydrochar samples

To observe the changes in the surface morphology of the hydrochars after alteration by HTC and the co-HTC processes, SEM images were captured. The SEM images (Fig. 2) showed that the surface morphology of the hydrochars were altered after the HTC and the co-HTC processes. Increasing the wt.% of JL appeared to have a co-HTC effect on the surface morphology of the hydrochars (Figs. 2d - 2f) with distinct surfaces. The increasing SSA (Fig. 3) due to the increasing wt.% of the JL and the change in feedstock compositions could be a contributing factor for the observed different surface morphology of the hydrochars. Notably, the 100 wt.% JL revealed the appearance of some visible porous pores likely due to its high SSA. These pores disappeared due to the co-HTC with the DM. The introduction of DM may have contributed to the blockage and reduction of the porous pores in the hydrochars from the co-HTC process. This could be said to conform with the results of the SSA and TPV. One of the possible reasons to the blockage of the porous pores could be due to the high ash content of the DM. It is well known that organic acids are formed because of the hydrolysis of biomass during HTC and catalyse the release of inorganic elements [15]. Given the low ash content of the JL (Table 1), this effect may not be noticeable as opposed to the co-HTC process with ash contribution by the DM. Another probable reason could be attributed to the adsorption of nitrogen from decomposed protein in DM on the porous surface of the hydrochars from the co-HTC process [28].

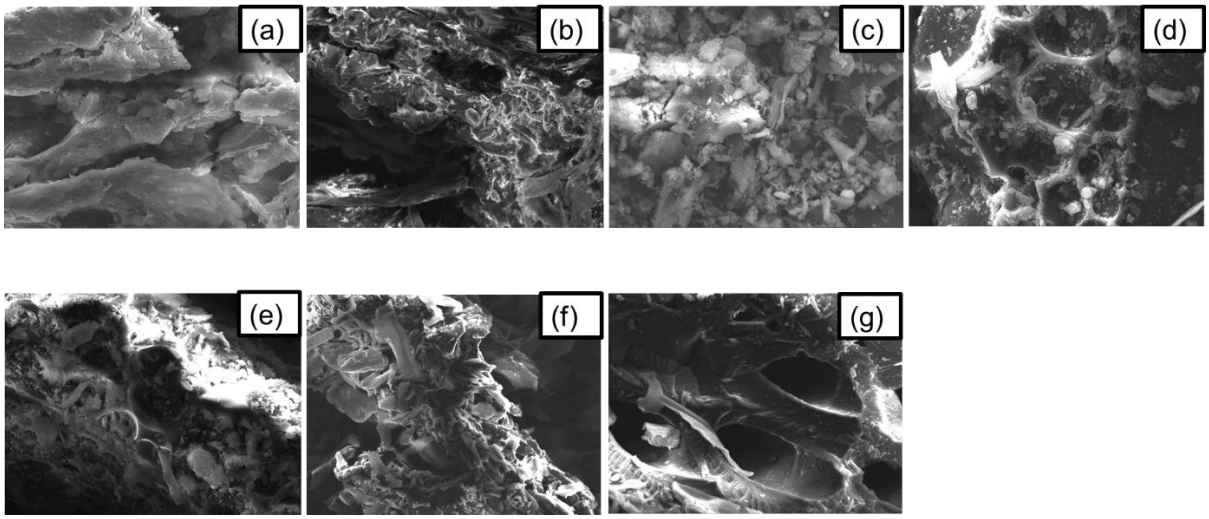

Fig. 2 captured SEM image at ×2000 magnification (a) Raw DM (b) Raw JL (C) 100 wt.% DM (d) 25 wt.% JL (e) 50 wt.% JL (f) 75wt.% JL and (g) 100 wt.% JL

3.6 Specific surface area, total pore volume and average pore diameter

To further verify the effect of the co-HTC process on the hydrochar morphology, the SSA, TPV and APD of the produced hydrochars were determined and depicted in Fig. 3. The 100 wt.% JL exhibited a high SSA and TPV likely due to its low ash content as previously stated. As a result of the co-HTC with a high ash DM, the SSA and TPV significantly declined. Hence, the implication would be that co-HTC of JL with a higher mass ratio of the DM may not facilitate high nutrient retention and better habitat for microbes if used for soil amendment [100]. Also, the surface may need some pre-treatment such as surface activation to increase its ability to adsorb contaminants from aqueous solutions [15]. However, the APD of all the hydrochars were nearly the same value.

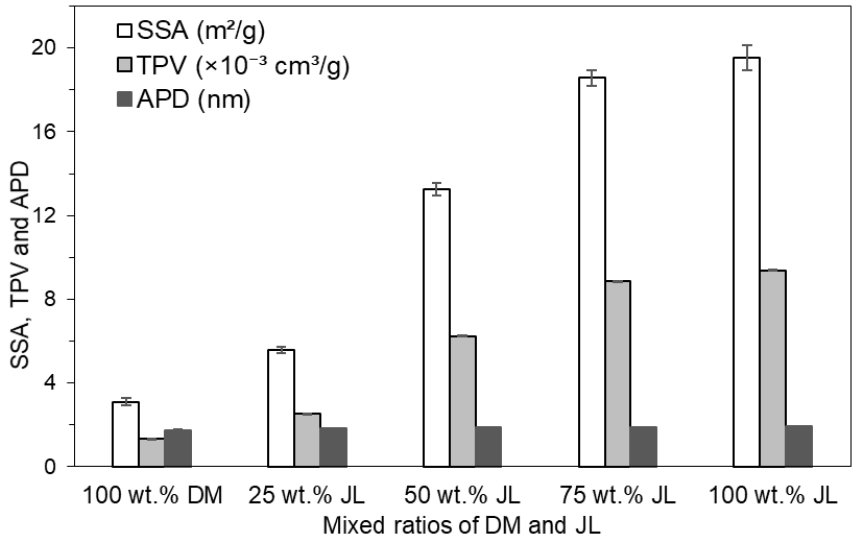

Fig. 3 specific surface area, total pore volume and average pore diameter

3.7 Changes in the functional groups of the hydrochar after HTC and co-HTC

To illustrate changes in the functional groups on the surface of the hydrochars at the different mixed ratio after co-HTC, FTIR analysis was performed and the result is presented in Fig. 4. The broad band of spectra observed between 3100 and 3500 cm^{-1} is ascribed to the stretching vibration of the −OH in the hydroxyl or carboxyl group [28, 84, 93]. Reduced peak intensities of the hydrochars between 3100 and 3500 cm^{-1} showed intensive dehydration reaction occurred during conversion at 260 °C [81, 84, 89, 93]. The stretching vibrations between 2870 and 2940 cm^{-1} showed the aliphatic $-CH_x$ group [84]. The stretching vibrations around 1645 cm^{-1} indicate the ketone and amide group of −C=O [84]. The peaks became slightly broader by co-HTC with the DM which showed that decarboxylation was promoted [84]. The sharp peaks observed between 2167 and 2297 cm^{-1} is ascribed to the −C≡N of the nitriles group [101]. The 100 wt.% JL showed no peek at this stretching vibration which indicates undetectable spectra of the −C≡N functional group. This could be related to the low nitrogen content of the JL (Table 1).

However, co-HTC with DM altered its functional group as peaks appeared thereafter. This revealed that there may have been a chemical interaction between the two biomasses and may have led to the formation of compounds linked to the −C≡N functional group. This could also be related to the captured SEM image (Figs. 2d, 2e and 2f) which showed no porous holes after the co-HTC process. The absence of peaks around 1735 cm^{-1} showed that hemicellulose was decomposed after the HTC and co-HTC processes at 260 °C. Certainly, Reza *et al*. [28] reported the absence of a peak at 1735 cm^{-1} after HTC pre-treatment of cow manure at 260 °C and was ascribed to the decomposition of hemicellulose. It is well known that hemicellulose decomposes completely after HTC pre-treatment of biomass at a temperature of 220 °C [37]. The finger prints vibrations between 1200 and 1460 cm^{-1} are ascribed to the degradation of lignocellulosic components [89, 93]. The sharp peaks observed at 1540 cm^{-1} was ascribed to increased lignin concentration [28]. Certainly, Reza *et al*. [28] observed that the lignin concentration in cow manure increased after HTC pre-treatment at 260 °C. The intense unstable vibrations between 870 and 1200 cm^{-1} are ascribed to the presence of mineral components or ash [93, 102, 103]. The sharp peaks observed for 100 wt.% DM and 25 wt.% JL could be due to the high ash composition (Table 1) at these mixed ratios. The peaks around 750 cm^{-1} suggests increased aromaticity of the hydrochars [81, 101].

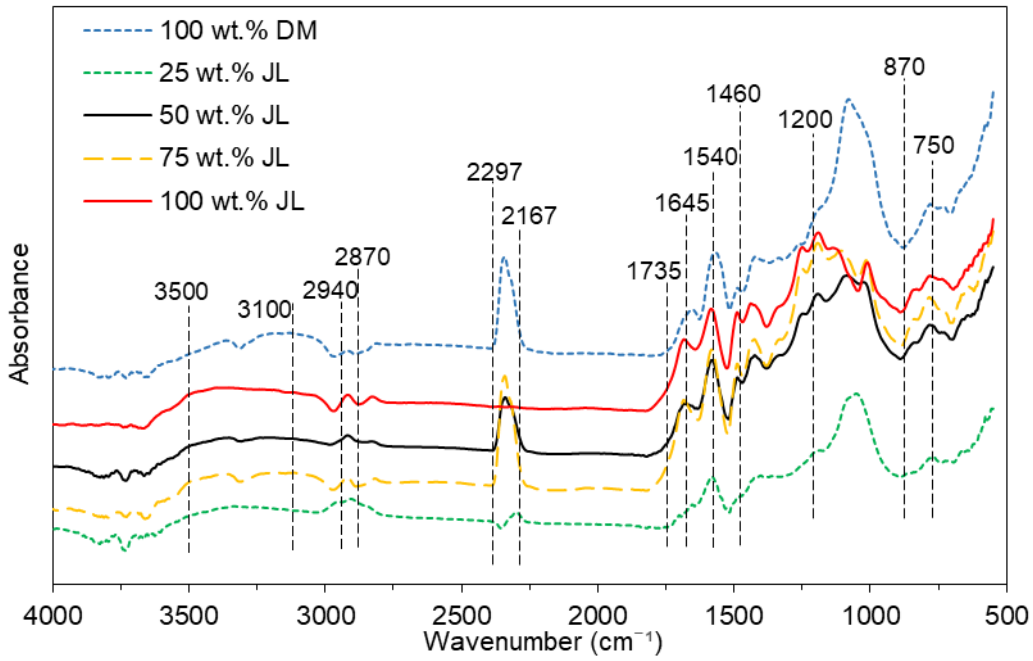

Fig. 4 the FTIR spectra of the hydrochars

3.8 Thermal behaviour and characteristic combustion parameters

Fig. 5 illustrates the mass loss (TG) and the derivative thermogravimetry (DTG) curves for the raw samples and the hydrochars at a heating rate of 10 °C/min (results for the other heating rates are shown in the appendices E-G). Some characteristic combustion temperatures were subsequently determined from the curves at the heating rate of 10 °C/min. The raw JL exhibited a further mass loss and DTG peaks than the DM (Fig. 5(a) and 5(b)). The further mass loss of the raw JL may have resulted from its higher VM and lower ash content (Table 1). Figs. 5(c) and 5(d) show the TG and DTG for the hydrochars. Fig. 5(d) revealed four distinctive peaks corresponding to the loss of moisture (50–200 °C), VM between 200–300 °C, organic matter of complex chemical structure, such as lignin combustion phase (300–400 °C), char combustion (400–600 °C) respectively [6, 81].

Table 2 depicts the characteristic temperatures, combustion parameters and performance of the hydrochars. The I_T is an important characteristic temperature to determine the probability of fire or explosion of a solid biofuel during storage and transportation [6]. A higher I_T is a desirable property of solid biofuel which means the difficulty of ignition, thus reduces the risk of fire or explosion [84]. The I_T of hydrochar is expected to change due to the changes in properties caused by hydrolysis, decarboxylation, dehydration, and aromatization reactions during conversion. The hydrochar blend ratio of 50 wt.% JL exhibited a slightly higher I_T after the co-HTC process probably due to its lower VM (Table 1). However, the I_T of the 100 wt.% JL was higher than those of the other hydrochars despite having a relatively higher VM. Certainly, He *et al*. [84] reported a similar observation where the I_T of the hydrochar from rice straws was higher than the those of the co-HTC process with a sewage sludge despite its higher VM of 42.7%. One of the probable reasons for the higher I_T of the 100 wt.% JL could be its distinct feedstock properties (being a woody biomass that is expected to be richer in lignocellulosic components) which does not contain the DM like the other samples. It is also clear from the FTIR result in Fig. 3 that the 100 wt.% JL did not show a peak for the −C≡N functional group which may probably have reduced its higher I_T and thermal stability. Indeed, Venna *et al*. [81] reported that the presence of degraded substances from protein in hydrochar could decrease its I_T and thermal stability. However, the higher I_T of the 100 wt.% JL showed that it is more thermally stable and will be safer than the other hydrochars during handling, storage, and transportation [83, 84].

The B_T is also a desirable property of solid biofuel; a high B_T implies a longer combustion process [84]. The blend ratio of 75 wt.% JL exhibited the lowest B_T of 504.8 °C which corresponds to its lowest B_t of 47.7 minutes compared to the other

hydrochars from the co-HTC process. A possible reason could be its lower ash content or R_m (Tables 1 and 2) compared to the other hydrochars from the co-HTC process. It was reported that inorganics in the ash can cause a decreased combustion reactivity of a solid biofuel [84]. Moreover, combustion is a complex reaction process and hence, different feedstocks have different combustion behaviour. In contrast, the highest B_T of 552.9 °C was observed for the 100 wt.% JL despite its low ash content. The observed B_T could also be related to the feedstock composition of the 100 wt.% JL as earlier explained. Moreover, this observation is also similar to the study by He *et al*. [84] where the B_T of the hydrochar produced from orange peels was higher than those of the co-HTC process with sewage sludge despite its lower ash content of 1.97%. As for the T_m, a closely similar trend to the B_T was observed. The R_m after combustion of raw feedstocks and the hydrochars are also shown in Table 2. A noticeable reduction in the R_m of the hydrochars was observed as the wt.% of JL was increased and followed a similar trend as the ash content (Table 1) determined using a furnace.

The CCI and CSI are also useful indicators to evaluate the combustion performance of a solid biofuel. The higher values of CCI and CSI indicate improved combustion performance and stability. It should be noted that these indices are dependent on the I_T, T_m, DTG_{max}, DTG_{av}, and B_T parameters. The CCI and CSI were lowered after the HTC process possibly owing to the reduced VM contents [84]. The decreased CCI and CSI values means a decrease in the combustion performance and stability of hydrochars after HTC pre-treatment. However, this could be an advantage during usage for combustion because heat loss could be reduced due to unstable flame that may result from high VM [84]. The lowest CCI and CSI values of 1.3 and 0.4 were determined for

the 100 wt.% JL due to its higher I_T, T_m and B_T which showed a decreased combustion performance [50] compared to the other hydrochars. Interestingly, the combustion performance of the co-HTC process improved at 75 wt.% JL and hence a positive synergy.

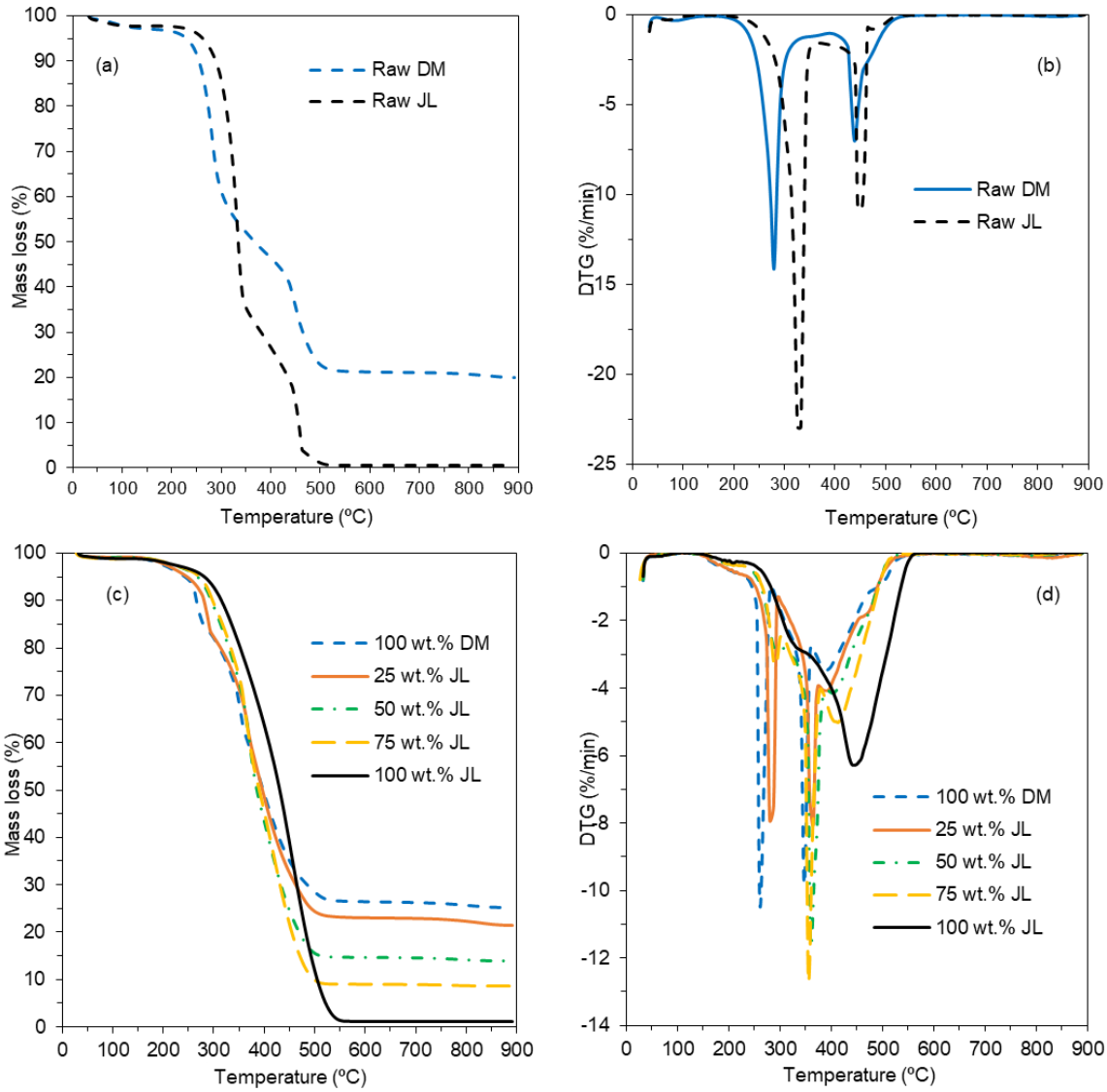

Fig. 5 (a) the mass loss for the raw samples (b) DTG for raw samples (c) the mass loss for the hydrochars (d) DTG for the hydrochars at a heating rate of 10 °C/min.

Table 2 Characteristic temperatures, combustion parameters and performance at 10 °C/min

Sample	I_T (°C)	DTG_{max} (%/min.)	DTG_{av} (%/min.)	B_T (°C)	B_t (min.)	T_m (°C)	R_m (%)	CCI ($10^{-7}\times min^{-2}\times C^{-3}$)	CSI ($10^4 \times min^{-1}\times C^{-2}$)
Raw DM	234.4	14.2	0.91	534.5	50.9	283.2	19.9	4.4	1.8
Raw JL	268.0	22.9	1.13	515.5	48.6	322.0	0.61	6.9	2.3
100wt.% DM	239.3	10.4	0.85	513.3	48.6	259.9	25.1	3.0	1.4
25wt.% JL	263.3	8.0	0.89	508.5	48.2	364.5	21.4	2.0	7.2
50wt.% JL	273.4	11.5	0.98	508.5	48.2	359.4	13.9	2.9	1.0
75wt.% JL	272.9	12.7	1.04	504.8	47.7	356.3	8.7	3.5	1.1
100wt.% JL	316.2	6.3	1.13	552.9	52.7	444.5	1.2	1.3	0.4

3.9 Activation energy of the raw samples and the hydrochars

Figs. 6 and 7 show the plots of $\ln \beta$ and $\ln\left(\frac{\beta}{T^2}\right)$ versus 1/T at the heating rates of 5, 10, 15 and 20 °C/min for the FWO and KAS models, respectively. The slopes and the intercepts at each α of 0.1 to 0.8 from simple regression line equations or plots were used to determine the activation energies of the samples (appendices H and I). Tables 3 and 4 show the activation energies and their respective coefficients of determinations (R^2) for the raw samples and the hydrochars from the HTC and the co-HTC processes, respectively. The average determined activation energy values of 72.1 and 69.7 kJ mol^{-1} for the raw JL by the FWO and KAS models were higher than 50.5 and 47.3 kJ mol^{-1} for the raw DM. This means that more energy could be required to break the bonds in the biomass matrix to initiate the combustion process of the raw JL than the raw DM [6, 50], which successfully explained the higher ignition temperature of the raw JL than the raw DM (Table 2). The average activation energies of the hydrochars from the HTC process (Table 3) decreased for the FWO and KAS models. The decreased activation is reported to be partly caused by the hydrochar properties such as highly amorphous carbonaceous structure and high surface area [6]. As for the co-HTC process, the average activation energies of the hydrochars (Table 4) also decreased except at 50 wt.% JL for the FWO

and KAS models. The hydrochar of 50 wt.% JL revealed a higher determined activation energy value of 55.2 and 51.7 kJ mol^{-1} for the FWO and KAS models. This suggests that it could be more resistant to thermal decomposition than the other hydrochars [6]. One of the probable reasons could be that, at 50 wt.% JL (equal wt.% of the JL and DM), there was a higher possibility for more equilibrium in chemical interaction between the feedstocks during conversion. The equilibrium in interaction during conversion may have enhanced polymerization and aromatization reactions which may have led to the formation of a more thermal resistant hydrochar, resulting in higher activation energy.

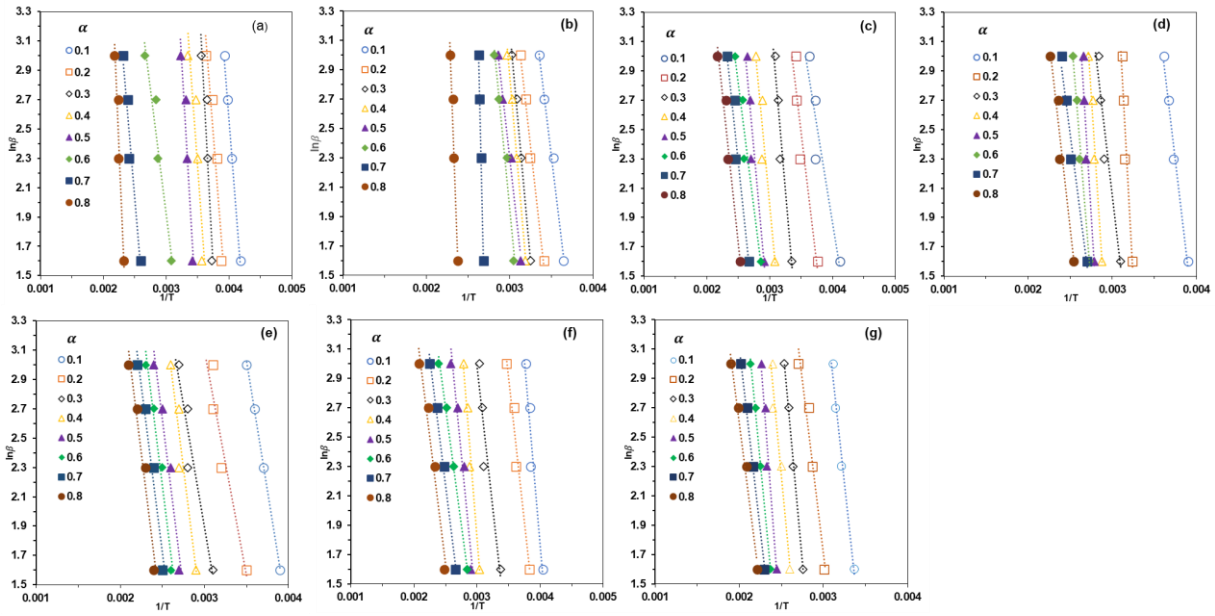

Fig. 6 the kinetic plots for the FWO, (a) raw DM (b) raw JL (c) 25 wt.% JL (d) 50 wt.% JL (e) 75 wt.% JL (f) 100 wt.% DM (g) 100 wt.% JL

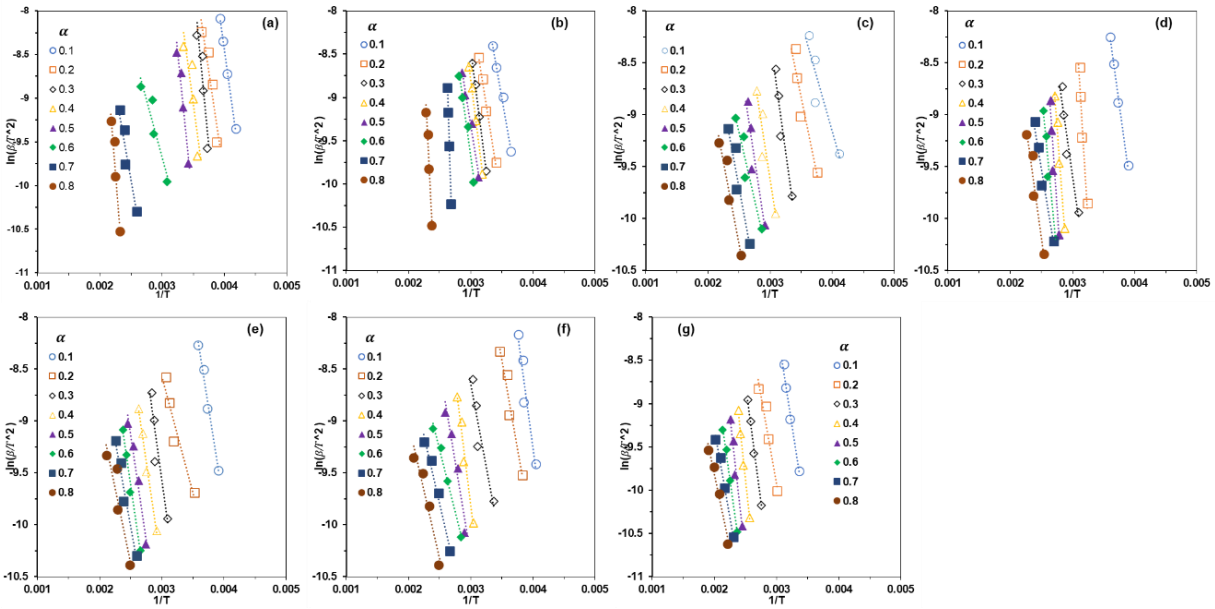

Fig. 7 the kinetic plots for the KAS, (a) raw DM (b) raw JL (c) 25 wt.% JL (d) 50 wt.% JL (e) 75 wt.% JL (f) 100 wt.% DM (g) 100 wt.% JL

Table 3 Activation energies for the raw samples and hydrochars from the HTC process at 10 °C/min

Sample	α	FWO		Sample	α	KAS	
		E_a (kJ mol^{-1})	R^2			E_a (kJ mol^{-1})	R^2
Raw DM	0.1	43.9	0.995	Raw DM	0.1	41.8	0.995
	0.2	43.6	0.896		0.2	41.1	0.872
	0.3	64.3	0.861		0.3	62.4	0.838
	0.4	46.4	0.830		0.4	43.5	0.792
	0.5	60.5	0.943		0.5	58.1	0.929
	0.6	26.7	0.930		0.6	22.0	0.886
	0.7	39.4	0.939		0.7	34.3	0.913
	0.8	79.4	0.918		0.8	75.3	0.898
	Average	50.5	0.914		Average	47.3	0.890
Raw JL	0.1	37.4	0.989	Raw JL	0.1	34.3	0.987
	0.2	39.8	0.986		0.2	36.5	0.981
	0.3	50.4	0.995		0.3	47.3	0.992
	0.4	51.1	0.955		0.4	47.9	0.992
	0.5	39.9	0.987		0.5	36.1	0.983
	0.6	45.8	0.971		0.6	42.2	0.963
	0.7	192.5	0.998		0.7	194.9	0.998
	0.8	120.1	0.958		0.8	118.1	0.949
	Average	72.1	0.979		Average	69.7	0.981
100 wt.% DM	0.1	39.4	0.928	100 wt.% DM	0.1	36.9	0.909
	0.2	31.1	0.959		0.2	27.9	0.942
	0.3	30.6	0.903		0.3	26.7	0.868
	0.4	43.9	0.975		0.4	40.2	0.966
	0.5	34.7	0.959		0.5	30.1	0.938
	0.6	25.2	0.994		0.6	19.9	0.986
	0.7	27.3	0.989		0.7	21.7	0.977
	0.8	27.6	0.963		0.8	21.5	0.928
	Average	32.5	0.959		Average	28.1	0.939
100 wt.% JL	0.1	42.4	0.979	100 wt.% JL	0.1	39.1	0.975
	0.2	37.5	0.954		0.2	33.2	0.933
	0.3	50.4	0.996		0.3	46.3	0.994
	0.4	48.9	0.955		0.4	56.9	0.979
	0.5	59.8	0.952		0.5	55.4	0.939
	0.6	47.8	0.995		0.6	42.5	0.992
	0.7	39.9	0.995		0.7	33.9	0.989
	0.8	35.6	0.986		0.8	29.0	0.975
	Average	45.3	0.977		Average	42.1	0.972

Table 4 Activation energies for the hydrochar from the co-HTC process at 10 °C/min

Sample	α	FWO		Sample	α	KAS	
		E_α (kJ mol^{-1})	R^2			E_α (kJ mol^{-1})	R^2
25 wt.% JL	0.1	21.1	0.883	25 wt.% JL	0.1	17.7	0.829
	0.2	28.1	0.903		0.2	24.7	0.870
	0.3	40.4	0.941		0.3	37.0	0.925
	0.4	36.4	0.911		0.4	32.3	0.877
	0.5	37.1	0.898		0.5	32.7	0.862
	0.6	26.5	0.943		0.6	21.4	0.906
	0.7	32.2	0.939		0.7	26.9	0.903
	0.8	31.8	0.959		0.8	26.1	0.931
	Average	31.7	0.922		Average	27.4	0.888
50 wt.% JL				50 wt.% JL			
	0.1	38.4	0.989		0.1	35.7	0.987
	0.2	84.6	0.908		0.2	83.1	0.897
	0.3	38.9	0.926		0.3	35.1	0.905
	0.4	70.7	0.969		0.4	67.8	0.961
	0.5	76.6	0.917		0.5	73.9	0.906
	0.6	55.9	0.974		0.6	52.1	0.966
	0.7	35.9	0.969		0.7	30.9	0.957
	0.8	40.4	0.954		0.8	35.2	0.931
	Average	55.2	0.951		Average	51.7	0.939
75 wt.% JL	0.1	27.9	0.998	75 wt.% JL	0.1	31.4	0.987
	0.2	24.3	0.921		0.2	18.7	0.904
	0.3	26.3	0.909		0.3	35.7	0.859
	0.4	36.6	0.926		0.4	33.6	0.977
	0.5	36.4	0.962		0.5	33.8	0.971
	0.6	36.4	0.962		0.6	33.9	0.986
	0.7	36.4	0.962		0.7	27.4	0.962
	0.8	36.4	0.962		0.8	23.9	0.869
	Average	32.6	0.950		Average	29.8	0.939

3.10 Thermodynamic analysis

The thermodynamic parameters of thermal decomposition are of great importance to properly design a combustion equipment [2, 6]. Table 5 showed the thermodynamic properties of activation for the raw samples and the hydrochars. In general, the value of $A < 10^9$ s^{-1} shows a surface reaction in most cases [96]. The average value of A from Table 5 varied from 10^2 to 10^7 for the FWO and KAS models. The values of A suggested that complex reactions occurred during the thermal degradation process [3,37].

A positive value of $\Delta G^{\ddagger}$ for a process means it is non-spontaneous while a negative value means it is spontaneous [2, 6, 96]. A spontaneous process does not require external energy for initiation while a non-spontaneous process such as solid fuel combustion needs energy supply to initiate the process. The positive values of $\Delta G^{\ddagger}$ observed in Table 5 revealed that the thermal degradation of the samples was not a spontaneous process [2, 104]. This means that energy must be supplied to initiate the combustion process of the raw samples and the hydrochars. The hydrochars from the co-HTC process have lower $\Delta G^{\ddagger}$ values than the 100 wt.% JL but higher $\Delta G^{\ddagger}$ values than for the 100 wt.% DM. This suggests that the combustion process of the hydrochars from the co-HTC is more favored compared to the 100 wt.% JL but less favored compared to the 100 wt.% DM [6].

The $\Delta H^{\ddagger}$ value is reported to be a better parameter for predicting the bond strength than the E_a value [6]. The values of $\Delta H^{\ddagger}$ followed a similar trend like those of the average values of E_a (Tables 3,4 and 5). Moreover, it was also reported that if the difference between the value of $\Delta H^{\ddagger}$ and E_a is small (in this case, the differences from Table 5 were < 6 kJ mol^{-1}) then, a low energy barrier would be needed to promote the formation of the activated complex of the sample [6, 104]. Lang *et al*. [6] also reported a similar trend (< 7 kJ mol^{-1} between $\Delta H^{\ddagger}$ and E_a values) from the

combustion of hydrochar from the co-HTC process and concluded that a low energy barrier was needed. In addition, the positive $\Delta H^{\ddagger}$ values in Table 5 means endothermicity of the process which suggests that, to overcome the activation barrier, energy need to be supplied for the thermal degradation of the samples for both the FWO and KAS kinetic models [96]. The result showed that the raw JL needed a higher energy supply (67.0 and 64.6 kJ mol^{-1}) to overcome the activation barrier to promote its transformation during combustion than the raw DM by both FWO and KAS models. For the HTC process, 100 wt.% JL was the most difficult to proceed with its combustion process during transformation. As for the co-HTC process, 50 wt.% JL has the highest value of $\Delta H^{\ddagger}$ (49.9 and 46.5 kJ mol^{-1}) which means that it is more difficult to initiate its combustion process to the transition state. The 25 wt.% JL is the easiest to initiate its combustion process because it needs the lowest external energy supply to overcome the activation barrier and hence, accelerated combustion ($\Delta H^{\ddagger}$= 26.5 kJ mol^{-1}).

The value of $\Delta S^{\ddagger}$ for a process showed the degree of randomness or disorder of matter and energy in the system or process [2, 6, 96]. A high value of $\Delta S^{\ddagger}$ for a process or system implies that, it is in a state further from thermodynamic equilibrium, showing high reactivity [2, 6, 96]. Therefore, the sample with a higher value of $\Delta S^{\ddagger}$, required more energy to reduce the degree of disorder during transformation [2, 6]. The low values of $\Delta S^{\ddagger}$ from Table 5 showed that the degree of disorder of matter was low during transformation. Results from this study in Table 5 showed that the degree of disorder decreased after the HTC and co-HTC processes (lower values than the raw samples). The lowest degree of randomness of −201.6 and −209.6 J mol^{-1} were observed for 25 wt.% JL which depicts lower reactivity during transformation by thermal degradation [2]. On the other hand, the 50 wt.% JL exhibits the highest degree of randomness (−159.4 and −165.3 J

mol^{-1}) compared to the other hydrochars which suggests higher reactivity [6]. Low values of $\Delta S^{\ddagger}$ < 0 have been previously reported for the combustion of hydrochar from a co-HTC of corn stalks and swine manure [6]. In addition, since combustion is a complex process, it is obvious from Table 5 that the observed differences could be attributed to the material or feedstock composition and the method used to calculate the parameters.

Table 5 Thermodynamic analysis values at 10 °C/min

	Sample	A (s^{-1})	$\Delta G^{\ddagger}$ (kJ mol^{-1})	$\Delta H^{\ddagger}$ (kJ mol^{-1})	$\Delta S^{\ddagger}$ (J mol^{-1})
FWO	Raw DM	3.09×10^{5}	131.2	45.6	−153.9
	Raw JL	1.48×10^{7}	139.6	67.0	−121.9
	100 DM	5.91×10^{3}	127.1	27.3	−187.2
	25 wt.% JL	1.04×10^{3}	155.0	26.5	−201.6
	50 wt.% JL	1.69×10^{5}	150.7	49.9	−159.4
	75 wt.% JL	1.41×10^{3}	152.7	27.3	−199.2
	100 wt.% JL	5.91×10^{3}	174.5	39.6	−187.9
KAS	Raw DM	1.45×10^{5}	131.5	42.4	−160.2
	Raw JL	8.69×10^{6}	139.8	64.6	−126.2
	100 DM	1.91×10^{3}	127.8	22.9	−196.6
	25 wt.% JL	3.99×10^{2}	155.8	22.2	−209.6
	50 wt.% JL	8.25×10^{4}	151.1	46.5	−165.3
	75 wt.% JL	7.59×10^{2}	153.2	24.5	−204.4
	100 wt.% JL	3.21×10^{3}	174.9	36.4	−192.9

4 Conclusion

Co-HTC was used to upgrade the solid biofuel quality indices of hydrochar from a blend of DM and JL. The produced hydrochars showed a promising property closed to the coal. An increase in the fixed carbon and carbon contents were observed as the mass ratio of the JL was increased. The blend of 75 wt.% JL had the lowest ash content of 7.2±0.5% compared to the other blends. The HHV of hydrochars improved remarkably to 26.4±0.02 as the ratio of JL in the mixture was increased. The surface morphology and the surface functional groups were altered by the co-HTC process. Surface characteristics such as SSA and TPV were also significantly increased after the co-HTC process. Thermal behaviour also revealed an improvement in combustion characteristics of the hydrochars. A decline in the combustion performance was observed after the HTC process

but improved at 75 wt.% JL after the co-HTC process. The kinetic analysis also revealed that the activation energy decreased after the HTC process but increased to a higher value at 50 wt.% JL after the co-HTC process. Therefore, hydrochar production by co-HTC of DM and JL has proved to be an effective and promising solid biofuel source.

Acknowledgement

The authors acknowledge the Instrumental Analyses Division of Hokkaido University, Japan, for performing elemental analyses of the samples. The authors also acknowledge Associate Professor Takahiro Nomura and Dr. Ade Kurniawan of the Centre for Advanced Research of Energy and Materials, Faculty of Engineering, Hokkaido University, Japan, for granting permission and assistance in performing the thermal analyses and surface morphology (SEM) in its laboratory.

Declarations

Funding Not applicable.

Conflicts of interest The authors declare that they have no known competing interests.

Data availability Supplementary data is available.

Code availability Not applicable

CHAPTER 5

5.0 CONCLUDING SUMMARY AND RECOMMENDATION

5.1 General conclusion

In the first phase of this study, hydrochar from dairy manure (DM) was produced by progressively reducing the quantity of water needed for conversion. Hence, the hypothesis that hydrochar with improved fuel properties would be produced from low moisture content biomass without the need to add water was investigated. To verify the hypothesis, DM was hydrothermally pre-treated at high and low moisture conditions. The low and high moisture content conditions were classified as the liquid-based HTC (L-HTC) and the vapor-based HTC (V-HTC). The results showed that the V-HTC process decomposed biomass better than the L-HTC process, hence, improved the fuel properties of DM. The V-HTC process is conducted at a higher B/W ratio, where the lower liquid content is small and may facilitate the formation of secondary char on the hydrochar surface and increase the severity of the reaction due to the higher acid content (due to the increased feedstock concentration), resulting in higher energy densification and mass yield. As a result, the V-HTC process is expected to have a higher hydrochar production capacity since less water is used compared to the L-HTC process. The proximate compositions showed that the ash content reached the maximum at B/W ratios of 0.43 and 0.67 rather than 1.0, and thus further studies are required to understand this behaviour. The obtained results nonetheless support the hypothesis of the study. This study showed that hydrochar with improved fuel properties can be produced from low moisture content biomass in HTC without the need for excess water.

The second phase of the study involves conducting a co-hydrothermal (co-HTC) of the DM and the Japanese larch (JL) due to the high ash properties of the DM. Hence, co-HTC was used to

upgrade the solid biofuel quality indices of hydrochar from the blend of DM and JL. The produced hydrochars showed a promising property closed to the coal. An increase in the fixed carbon and carbon contents were observed as the mass ratio of the JL was increased. The blend of 75 wt.% JL had the lowest ash content of 7.2±0.5% compared to the other blends. The HHV of hydrochars improved to 25.1±0.02 and 26.4±0.02 as the mixture was increased to 50 and 75 wt.% JL. The surface morphology and the surface functional groups were altered by the co-HTC process. Surface characteristics such as SSA and TPV were also significantly increased after the co-HTC process. Thermal behaviour also revealed an improvement in combustion characteristics of the hydrochars. A decline in the combustion performance was observed after the HTC process but improved at 75 wt.% JL after the co-HTC process. The kinetic analysis also revealed that the activation energy decreased after the HTC process but increased to a higher value at 50 wt.% JL after the co-HTC process. Therefore, hydrochar production by co-HTC of DM and JL has proved to be an effective and promising solid biofuel source.

Conclusively, for a sustainable production of hydrochar with less negative environmental impact from HTC waste stream, this study recommends that HTC should be conducted using high B/W ratio of 1.0. In addition, to avoid the problems of fouling and slagging tendency in a combustion equipment due to the high ash content from solid biofuel produced from DM, co-HTC technique with a low ash content lignocellulosic biomass should employed.

5.2 Recommendations

- Proximate analysis revealed that the ash content was maximum at B/W ratios of 0.43 and 0.67 rather than 1.0, and thus further studies are required to understand this behaviour.

- Further study is also required to compare the present findings from this study to the other available systems for conducting the V-HTC with the same feedstock and process variables.

REFERENCES

1. Basu P (2013) Biomass Gasification, Pyrolysis and Torrefaction. 2nd ed. Elsevier. https://doi.org/10.1016/C2011-0-07564-6.

2. Chen J, Wang Y, Lang X, et al (2017) Evaluation of agricultural residues pyrolysis under non-isothermal conditions: Thermal behaviors, kinetics, and thermodynamics. Bioresource Technology 241:340–348. https://doi.org/10.1016/j.biortech.2017.05.036

3. Field CB, Campbell JE, Lobell DB (2008) Biomass energy: the scale of the potential resource. Trends in Ecology and Evolution 23:65–72. https://doi.org/10.1016/J.TREE.2007.12.001

4. Martins F, Felgueiras C, Smitkova M, Caetano N (2019) Analysis of Fossil Fuel Energy Consumption and Environmental Impacts in European Countries. Energies 2019, Vol 12, Page 964 12:964. https://doi.org/10.3390/EN12060964

5. Kambo HS, Dutta A (2015) A comparative review of biochar and hydrochar in terms of production, physico-chemical properties and applications. Renewable and Sustainable Energy Reviews 45:359–378. https://doi.org/10.1016/j.rser.2015.01.050

6. Lang Q, Zhang B, Liu Z, et al (2019) Co-hydrothermal carbonization of corn stalk and swine manure: Combustion behavior of hydrochar by thermogravimetric analysis. Bioresource Technology 271:75–83. https://doi.org/10.1016/j.biortech.2018.09.100

7. Cárdenas-Aguiar E, Gascó G, Paz-Ferreiro J, Méndez A (2019) Thermogravimetric analysis and carbon stability of chars produced from slow pyrolysis and hydrothermal carbonization of manure waste. Journal of Analytical and Applied Pyrolysis 140:434–443. https://doi.org/10.1016/J.JAAP.2019.04.026

8. Shimahata A, Farghali M, Fujii M (2020) Factors Influencing the Willingness of Dairy Farmers to Adopt Biogas Plants: A Case Study in Hokkaido, Japan. Sustainability 2020, Vol 12, Page 7809 12:7809. https://doi.org/10.3390/SU12187809

9. Wu K, Gao Y, Zhu G, et al (2017) Characterization of dairy manure hydrochar and aqueous phase products generated by hydrothermal carbonization at different temperatures. Journal of Analytical and Applied Pyrolysis 127:335–342. https://doi.org/10.1016/j.jaap.2017.07.017

10. Bach QV, Tran KQ, Khalil RA, et al (2013) Comparative assessment of wet torrefaction. Energy and Fuels 27:6743–6753. https://doi.org/10.1021/ef401295w

11. Bach QV, Skreiberg O (2016) Upgrading biomass fuels via wet torrefaction: A review and comparison with dry torrefaction. Renewable and Sustainable Energy Reviews 54:665–677. https://doi.org/10.1016/J.RSER.2015.10.014

12. Li Q, Zhang S, Gholizadeh M, et al (2021) Co-hydrothermal carbonization of swine and chicken manure: Influence of cross-interaction on hydrochar and liquid characteristics.

Science of The Total Environment 786:147381. https://doi.org/10.1016/J.SCITOTENV.2021.147381

13. Reza MT, Andert J, Wirth B, et al (2014) Hydrothermal Carbonization of Biomass for Energy and Crop Production. Applied Bioenergy 1:11–29. https://doi.org/10.2478/apbi-2014-0001

14. Shen Y (2020) A review on hydrothermal carbonization of biomass and plastic wastes to energy products. Biomass and Bioenergy 134:105479. https://doi.org/10.1016/J.BIOMBIOE.2020.105479

15. Fang J, Zhan L, Ok YS, Gao B (2018) Minireview of potential applications of hydrochar derived from hydrothermal carbonization of biomass. Journal of Industrial and Engineering Chemistry 57:15–21. https://doi.org/10.1016/j.jiec.2017.08.026

16. Antero RVP, Alves ACF, de Oliveira SB, et al (2020) Challenges and alternatives for the adequacy of hydrothermal carbonization of lignocellulosic biomass in cleaner production systems: A review. Journal of Cleaner Production 252:119899. https://doi.org/10.1016/j.jclepro.2019.119899

17. Kambo HS, Minaret J, Dutta A (2018) Process Water from the Hydrothermal Carbonization of Biomass: A Waste or a Valuable Product? Waste and Biomass Valorization 9:1181–1189. https://doi.org/10.1007/s12649-017-9914-0

18. Shafie SA, Al-attab KA, Zainal ZA (2018) Effect of hydrothermal and vapothermal carbonization of wet biomass waste on bound moisture removal and combustion characteristics. Applied Thermal Engineering 139:187–195. https://doi.org/10.1016/j.applthermaleng.2018.02.073

19. Ro KS, Libra JA, Alvarez-Murillo A (2020) Comparative studies on water-and vapor-based hydrothermal carbonization: Process analysis. Energies 13:. https://doi.org/10.3390/en13215733

20. Wang Y, Li Y, Zhang Y, et al (2021) Hydrothermal carbonization of garden waste by pretreatment with anaerobic digestion to improve hydrohcar performance and energy recovery. Science of The Total Environment 151014. https://doi.org/10.1016/J.SCITOTENV.2021.151014

21. Arauzo PJ, Olszewski MP, Wang X, et al (2020) Assessment of the effects of process water recirculation on the surface chemistry and morphology of hydrochar. Renewable Energy 155:1173–1180. https://doi.org/10.1016/J.RENENE.2020.04.050

22. Aragon-Briceño C, Pożarlik A, Bramer E, et al (2022) Integration of hydrothermal carbonization treatment for water and energy recovery from organic fraction of municipal solid waste digestate. Renewable Energy 184:577–591. https://doi.org/10.1016/J.RENENE.2021.11.106

23. Heidari M, Salaudeen S, Dutta A, Acharya B (2018) Effects of Process Water Recycling and Particle Sizes on Hydrothermal Carbonization of Biomass. Energy & Fuels 32:11576–11586. https://doi.org/10.1021/ACS.ENERGYFUELS.8B02684

24. Wang R, Jin Q, Ye X, et al (2020) Effect of process wastewater recycling on the chemical evolution and formation mechanism of hydrochar from herbaceous biomass during hydrothermal carbonization. Journal of Cleaner Production 277:. https://doi.org/10.1016/J.JCLEPRO.2020.123281

25. Wang F, Wang J, Gu C, et al (2019) Effects of process water recirculation on solid and liquid products from hydrothermal carbonization of Laminaria. Bioresource Technology 292:121996. https://doi.org/10.1016/J.BIORTECH.2019.121996

26. Nobre C, Alves O, Durão L, et al (2021) Characterization of hydrochar and process water from the hydrothermal carbonization of Refuse Derived Fuel. Waste Management 120:303–313. https://doi.org/10.1016/J.WASMAN.2020.11.040

27. Gao Y, Liu Y, Zhu G, et al (2018) Microwave-assisted hydrothermal carbonization of dairy manure: Chemical and structural properties of the products. Energy 165:662–672. https://doi.org/10.1016/j.energy.2018.09.185

28. Reza MT, Freitas A, Yang X, et al (2016) Hydrothermal carbonization (HTC) of cow manure: Carbon and nitrogen distributions in HTC products. Environmental Progress & Sustainable Energy 35:1002–1011. https://doi.org/10.1002/EP.12312

29. Smith AM, Singh S, Ross AB (2016) Fate of inorganic material during hydrothermal carbonisation of biomass: Influence of feedstock on combustion behaviour of hydrochar. Fuel 169:135–145. https://doi.org/10.1016/J.FUEL.2015.12.006

30. Doshi V, Vuthaluru HB, Korbee R, Kiel JHA (2009) Development of a modeling approach to predict ash formation during co-firing of coal and biomass. Fuel Processing Technology 90:1148–1156. https://doi.org/10.1016/J.FUPROC.2009.05.019

31. Kamimoto M The Significance of Liquid Fuel Production from Woody Biomass. AIST TODAY.

32. McKendry P (2002) Energy production from biomass (part 1): overview of biomass. Bioresource Technology 83:37–46. https://doi.org/10.1016/S0960-8524(01)00118-3

33. Khosravi A, Zheng H, Liu Q, et al (2022) Production and characterization of hydrochars and their application in soil improvement and environmental remediation. Chemical Engineering Journal 430:133142. https://doi.org/10.1016/J.CEJ.2021.133142

34. Fang J, Liu Z, Luan H, et al (2021) Thermochemical liquefaction of cattle manure using ethanol as solvent: Effects of temperature on bio-oil yields and chemical compositions. Renewable Energy 167:32–41. https://doi.org/10.1016/J.RENENE.2020.11.033

35. Farzad S, Mandegari MA, Görgens JF (2016) A critical review on biomass gasification, co-gasification, and their environmental assessments. Biofuel Research Journal 3:483–495. https://doi.org/10.18331/BRJ2016.3.4.3

36. Funke A, Ziegler F (2010) Hydrothermal carbonization of biomass: A summary and discussion of chemical mechanisms for process engineering. Biofuels, Bioproducts and Biorefining 4:160–177. https://doi.org/10.1002/bbb.198

37. Heidari M, Dutta A, Acharya B, Mahmud S (2019) A review of the current knowledge and challenges of hydrothermal carbonization for biomass conversion. Journal of the Energy Institute 92:1779–1799. https://doi.org/10.1016/j.joei.2018.12.003

38. Yeoh K-H, Shafie SA, Al-attab KA, Zainal ZA (2018) Upgrading agricultural wastes using three different carbonization methods: Thermal, hydrothermal and vapothermal. Bioresource Technology 265:365–371. https://doi.org/10.1016/j.biortech.2018.06.024

39. Funke A, Reebs F, Kruse A (2013) Experimental comparison of hydrothermal and vapothermal carbonization. Fuel Processing Technology 115:261–269. https://doi.org/10.1016/j.fuproc.2013.04.020

40. Wang M, Zhang M, Chen X, et al (2022) Hydrothermal conversion of Chinese cabbage residue for sustainable agriculture: Influence of process parameters on hydrochar and hydrolysate. Science of The Total Environment 812:152478. https://doi.org/10.1016/J.SCITOTENV.2021.152478

41. Barskov S, Zappi M, Buchireddy P, et al (2019) Torrefaction of biomass: A review of production methods for biocoal from cultured and waste lignocellulosic feedstocks. Renewable Energy 142:624–642. https://doi.org/10.1016/J.RENENE.2019.04.068

42. Kumar A, Jones DD, Hanna MA (2009) Thermochemical Biomass Gasification: A Review of the Current Status of the Technology. Energies 2009, Vol 2, Pages 556-581 2:556–581. https://doi.org/10.3390/EN20300556

43. Insights into the evolution of chemical structures in lignocellulose and non-lignocellulose biowastes during hydrothermal carbonization (HTC) | Elsevier Enhanced Reader. https://reader.elsevier.com/reader/sd/pii/S001623611831559X?token=ACA226B754F4B6DBB40513B98CC7F86379BDE866745FB0D69B951110BB3E926DF23D48414D526F04889E475F68EF9466&originRegion=us-east-1&originCreation=20211104153203. Accessed 5 Nov 2021

44. Mettanant V, Basu P, Butler J (2009) Agglomeration of biomass fired fluidized bed gasifier and combustor. Canadian Journal of Chemical Engineering 87:656–684. https://doi.org/10.1002/CJCE.20211

45. Aragón-Briceño CI, Grasham O, Ross AB, et al (2020) Hydrothermal carbonization of sewage digestate at wastewater treatment works: Influence of solid loading on characteristics of hydrochar, process water and plant energetics. Renewable Energy 157:959–973. https://doi.org/10.1016/J.RENENE.2020.05.021

46. Lang Q, Liu Z, Li Y, et al (2021) Combustion characteristics, kinetic and thermodynamic analyses of hydrochars derived from hydrothermal carbonization of cattle manure. Journal of Environmental Chemical Engineering 106938. https://doi.org/10.1016/J.JECE.2021.106938

47. Parthasarathy P, Al-Ansari T, Mackey HR, McKay G (2021) Effect of heating rate on the pyrolysis of camel manure. Biomass Conversion and Biorefinery 2021 1–13. https://doi.org/10.1007/S13399-021-01531-9

48. Mureddu M, Dessì F, Orsini A, et al (2018) Air- and oxygen-blown characterization of coal and biomass by thermogravimetric analysis. Fuel 212:626–637. https://doi.org/10.1016/j.fuel.2017.10.005

49. Singh S, Sawarkar AN (2020) Thermal decomposition aspects and kinetics of pyrolysis of garlic stalk. https://doi.org/101080/1556703620201716891. https://doi.org/10.1080/15567036.2020.1716891

50. Qianqian Lang, Hainan Luo, Yi Li, et al (2019) Thermal behavior of hydrochar from co-hydrothermal carbonization of swine manure and sawdust: effect of process water recirculation. Sustainable Energy & Fuels 3:2329–2336. https://doi.org/10.1039/C9SE00332K

51. Fernandez-Lopez M, Pedrosa-Castro GJ, Valverde JL, Sanchez-Silva L (2016) Kinetic analysis of manure pyrolysis and combustion processes. Waste Management 58:230–240. https://doi.org/10.1016/J.WASMAN.2016.08.027

52. Al-Mulali U, Lee JY, Hakim Mohammed A, Sheau-Ting L (2013) Examining the link between energy consumption, carbon dioxide emission, and economic growth in Latin America and the Caribbean. Renewable and Sustainable Energy Reviews 26:42–48. https://doi.org/10.1016/J.RSER.2013.05.041

53. Lane DJ, Truong E, Larizza F, et al (2018) Effect of Hydrothermal Carbonization on the Combustion and Gasification Behavior of Agricultural Residues and Macroalgae: Devolatilization Characteristics and Char Reactivity. Energy and Fuels 32:4149–4159. https://doi.org/10.1021/acs.energyfuels.7b03125

54. Gascó G, Paz-Ferreiro J, Álvarez ML, et al (2018) Biochars and hydrochars prepared by pyrolysis and hydrothermal carbonisation of pig manure. Waste Management 79:395–403. https://doi.org/10.1016/j.wasman.2018.08.015

55. Wu K, Zhang X, Yuan Q (2018) Effects of process parameters on the distribution characteristics of inorganic nutrients from hydrothermal carbonization of cattle manure. Journal of Environmental Management 209:328–335. https://doi.org/10.1016/j.jenvman.2017.12.071

56. Font-Palma C (2019) Methods for the Treatment of Cattle Manure—A Review. C 5:27. https://doi.org/10.3390/c5020027

57. Heidari M, Salaudeen S, Dutta A, Acharya B (2018) Effects of Process Water Recycling and Particle Sizes on Hydrothermal Carbonization of Biomass. Energy and Fuels 32:11576–11586. https://doi.org/10.1021/acs.energyfuels.8b02684

58. Köchermann J, Görsch K, Wirth B, et al (2018) Hydrothermal carbonization: Temperature influence on hydrochar and aqueous phase composition during process water recirculation. Journal of Environmental Chemical Engineering 6:5481–5487. https://doi.org/10.1016/j.jece.2018.07.053

59. Stemann J, Putschew A, Ziegler F (2013) Hydrothermal carbonization: Process water characterization and effects of water recirculation. Bioresource Technology 143:139–146. https://doi.org/10.1016/j.biortech.2013.05.098

60. Minaret J, Dutta A (2016) Comparison of liquid and vapor hydrothermal carbonization of corn husk for the use as a solid fuel. Bioresource Technology 200:804–811. https://doi.org/10.1016/j.biortech.2015.11.010

61. Sabio E, Álvarez-Murillo A, Román S, Ledesma B (2016) Conversion of tomato-peel waste into solid fuel by hydrothermal carbonization: Influence of the processing variables. Waste Management 47:122–132. https://doi.org/10.1016/j.wasman.2015.04.016

62. Álvarez-Murillo A, Román S, Ledesma B, Sabio E (2015) Study of variables in energy densification of olive stone by hydrothermal carbonization. Journal of Analytical and Applied Pyrolysis 113:307–314. https://doi.org/10.1016/j.jaap.2015.01.031

63. Volpe M, Fiori L (2017) From olive waste to solid biofuel through hydrothermal carbonisation: The role of temperature and solid load on secondary char formation and hydrochar energy properties. Journal of Analytical and Applied Pyrolysis 124:63–72. https://doi.org/10.1016/j.jaap.2017.02.022

64. Sermyagina E, Saari J, Kaikko J, Vakkilainen E (2015) Hydrothermal carbonization of coniferous biomass: Effect of process parameters on mass and energy yields. Journal of Analytical and Applied Pyrolysis 113:551–556. https://doi.org/10.1016/j.jaap.2015.03.012

65. Kim H-J, Oh S-C (2021) Hydrothermal Carbonization of Spent Coffee Grounds. Applied Sciences 11:6542. https://doi.org/10.3390/app11146542

66. Zheng X, Chen W, Ying Z, et al (2020) Structure-Reactivity Correlations in Pyrolysis and Gasification of Sewage Sludge Derived Hydrochar: Effect of Hydrothermal Carbonization. Energy and Fuels 34:1965–1976. https://doi.org/10.1021/acs.energyfuels.9b04275

67. Itoh T, Iwabuchi K, Maemoku N, et al (2019) A new torrefaction system employing spontaneous self-heating of livestock manure under elevated pressure. Waste Management 85:66–72. https://doi.org/10.1016/j.wasman.2018.12.018

68. Chen X, Ma X, Peng X, et al (2018) Conversion of sweet potato waste to solid fuel via hydrothermal carbonization. Bioresource Technology 249:900–907. https://doi.org/10.1016/j.biortech.2017.10.096

69. Xie C, Liu J, Zhang X, et al (2018) Co-combustion thermal conversion characteristics of textile dyeing sludge and pomelo peel using TGA and artificial neural networks. Applied Energy 212:786–795. https://doi.org/10.1016/j.apenergy.2017.12.084

70. Nakason K, Panyapinyopol B, Kanokkantapong V, et al (2018) Hydrothermal carbonization of unwanted biomass materials: Effect of process temperature and retention time on hydrochar and liquid fraction. Journal of the Energy Institute 91:786–796. https://doi.org/10.1016/j.joei.2017.05.002

71. Cuvilas CA, Kantarelis E, Yang W (2015) The impact of a mild sub-critical hydrothermal carbonization pretreatment on Umbila wood. A mass and energy balance perspective. Energies 8:2165–2175. https://doi.org/10.3390/en8032165

72. Reza MT, Yan W, Uddin MH, et al (2013) Reaction kinetics of hydrothermal carbonization of loblolly pine. Bioresource Technology 139:161–169. https://doi.org/10.1016/j.biortech.2013.04.028

73. Lin Y, Ma X, Peng X, et al (2015) Effect of hydrothermal carbonization temperature on combustion behavior of hydrochar fuel from paper sludge. Applied Thermal Engineering 91:574–582. https://doi.org/10.1016/j.applthermaleng.2015.08.064

74. He C, Giannis A, Wang JY (2013) Conversion of sewage sludge to clean solid fuel using hydrothermal carbonization: Hydrochar fuel characteristics and combustion behavior. Applied Energy 111:257–266. https://doi.org/10.1016/j.apenergy.2013.04.084

75. He C, Zhang Z, Ge C, et al (2019) Synergistic effect of hydrothermal co-carbonization of sewage sludge with fruit and agricultural wastes on hydrochar fuel quality and combustion behavior. Waste Management 100:171–181. https://doi.org/10.1016/j.wasman.2019.09.018

76. Odeh AO (2015) Comprehensive Conventional Analysis of Southern Hemisphere Coal Chars of Different Ranks for Fixed Bed Gasification

77. Reza MT, Lynam JG, Uddin MH, Coronella CJ (2013) Hydrothermal carbonization: Fate of inorganics. Biomass and Bioenergy 49:86–94. https://doi.org/10.1016/J.BIOMBIOE.2012.12.004

78. Gao Y, Wang XH, Yang HP, Chen HP (2012) Characterization of products from hydrothermal treatments of cellulose. Energy 42:457–465. https://doi.org/10.1016/J.ENERGY.2012.03.023

79. Kim D, Lee K, Fuel KP-, 2014 undefined (2014) Hydrothermal carbonization of anaerobically digested sludge for solid fuel production and energy recovery. Elsevier 130:120–125. https://doi.org/10.1016/j.fuel.2014.04.030

80. Shen Y, Yu S, Ge S, et al (2017) Hydrothermal carbonization of medical wastes and lignocellulosic biomass for solid fuel production from lab-scale to pilot-scale. Energy 118:312–323. https://doi.org/10.1016/j.energy.2016.12.047

81. Venna S, Sharma HB, Reddy PHP, et al (2021) Landfill leachate as an alternative moisture source for hydrothermal carbonization of municipal solid wastes to solid biofuels. Bioresource Technology 320:124410. https://doi.org/10.1016/j.biortech.2020.124410

82. Xu M, fuels CS-E&, 2012 undefined (2012) Influences of the heat-treatment temperature and inorganic matter on combustion characteristics of cornstalk biochars. ACS Publications 26:209–218. https://doi.org/10.1021/ef2011657

83. Zhuang X, Zhan H, Huang Y, et al (2018) Conversion of industrial biowastes to clean solid fuels via hydrothermal carbonization (HTC): Upgrading mechanism in relation to coalification process and. Elsevier 267:17–29. https://doi.org/10.1016/j.biortech.2018.07.002

84. He C, Zhang Z, Ge C, et al (2019) Synergistic effect of hydrothermal co-carbonization of sewage sludge with fruit and agricultural wastes on hydrochar fuel quality and combustion behavior. Waste Management 100:171–181. https://doi.org/10.1016/J.WASMAN.2019.09.018

85. Lee J, Sohn D, Lee K, Park KY (2019) Solid fuel production through hydrothermal carbonization of sewage sludge and microalgae Chlorella sp. from wastewater treatment plant. Chemosphere 230:157–163. https://doi.org/10.1016/J.CHEMOSPHERE.2019.05.066

86. Mazumder S, Saha P, Reza MT (2020) Co-hydrothermal carbonization of coal waste and food waste: fuel characteristics. Biomass Conversion and Biorefinery 2020 1–11. https://doi.org/10.1007/S13399-020-00771-5

87. Liang M, Zhang K, Lei P, et al (2019) Fuel properties and combustion kinetics of hydrochar derived from co-hydrothermal carbonization of tobacco residues and graphene oxide. Biomass Conversion and Biorefinery 2019 10:1 10:189–201. https://doi.org/10.1007/S13399-019-00408-2

88. Bardhan M, Novera TM, Tabassum M, et al (2021) Co-hydrothermal carbonization of different feedstocks to hydrochar as potential energy for the future world: A review. Journal of Cleaner Production 298:126734. https://doi.org/10.1016/J.JCLEPRO.2021.126734

89. Lang Q, Guo Y, Zheng Q, et al (2018) Co-hydrothermal carbonization of lignocellulosic biomass and swine manure: Hydrochar properties and heavy metal transformation behavior. Bioresource Technology 266:242–248. https://doi.org/10.1016/J.BIORTECH.2018.06.084

90. Itoh T, Fujiwara N, Iwabuchi K, et al (2020) Effects of pyrolysis temperature and feedstock type on particulate matter emission characteristics during biochar combustion. Fuel Processing Technology 204:106408. https://doi.org/10.1016/J.FUPROC.2020.106408

91. Yuan X, He T, Cao H, Yuan Q (2017) Cattle manure pyrolysis process: Kinetic and thermodynamic analysis with isoconversional methods. Renewable Energy 107:489–496. https://doi.org/10.1016/J.RENENE.2017.02.026

92. Lu X, Yamauchi K, Phaiboonsilpa N, Saka S (2009) Two-step hydrolysis of Japanese beech as treated by semi-flow hot-compressed water. Journal of Wood Science 2009 55:5 55:367–375. https://doi.org/10.1007/S10086-009-1040-6

93. Zhang X, Zhang L, Li A (2017) Hydrothermal co-carbonization of sewage sludge and pinewood sawdust for nutrient-rich hydrochar production: Synergistic effects and products characterization. Journal of Environmental Management 201:52–62. https://doi.org/10.1016/J.JENVMAN.2017.06.018

94. Chen X, Ma X, Peng X, et al (2018) Conversion of sweet potato waste to solid fuel via hydrothermal carbonization. Bioresource Technology 249:900–907. https://doi.org/10.1016/J.BIORTECH.2017.10.096

95. Wang T, Zhai Y, Li H, et al (2018) Co-hydrothermal carbonization of food waste-woody biomass blend towards biofuel pellets production. Bioresource Technology 267:371–377. https://doi.org/10.1016/J.BIORTECH.2018.07.059

96. Ma J, Luo H, Li Y, et al (2019) Pyrolysis kinetics and thermodynamic parameters of the hydrochars derived from co-hydrothermal carbonization of sawdust and sewage sludge using thermogravimetric analysis. Bioresource Technology 282:133–141. https://doi.org/10.1016/J.BIORTECH.2019.03.007

97. Zhao P, Shen Y, Ge S, Yoshikawa K (2014) Energy recycling from sewage sludge by producing solid biofuel with hydrothermal carbonization. Energy Conversion and Management 78:815–821. https://doi.org/10.1016/J.ENCONMAN.2013.11.026

98. Zornoza R, Moreno-Barriga F, Acosta JA, et al (2016) Stability, nutrient availability and hydrophobicity of biochars derived from manure, crop residues, and municipal solid waste for their use as soil amendments. Chemosphere 144:122–130. https://doi.org/10.1016/J.CHEMOSPHERE.2015.08.046

99. Vassilev S v., Baxter D, Andersen LK, Vassileva CG (2010) An overview of the chemical composition of biomass. Fuel 89:913–933. https://doi.org/10.1016/J.FUEL.2009.10.022

100. Piash MI, Iwabuchi K, Itoh T, Uemura K (2021) Release of essential plant nutrients from manure- and wood-based biochars. Geoderma 397:115100. https://doi.org/10.1016/j.geoderma.2021.115100

101. Infrared Tables (short summary of common absorption... - Google Scholar. https://scholar.google.com/scholar?hl=en&as_sdt=0%2C5&q=Infrared+Tables+%28short+summary+of+common+absorption+frequencies%29.+Course+Notes%2C+2620%2C+19+&btnG=. Accessed 17 Aug 2021

102. Xu ZX, Song H, Zhang S, et al (2019) Co-hydrothermal carbonization of digested sewage sludge and cow dung biogas residue: Investigation of the reaction characteristics. Energy 187:115972. https://doi.org/10.1016/J.ENERGY.2019.115972

103. Zheng C, Ma X, Yao Z, Chen X (2019) The properties and combustion behaviors of hydrochars derived from co-hydrothermal carbonization of sewage sludge and food waste. Bioresource Technology 285:121347. https://doi.org/10.1016/J.BIORTECH.2019.121347

104. Dhyani V, Kumar Awasthi M, Wang Q, et al (2018) Effect of composting on the thermal decomposition behavior and kinetic parameters of pig manure-derived solid waste. Bioresource Technology 252:59–65. https://doi.org/10.1016/J.BIORTECH.2017.12.083

APPENDICES

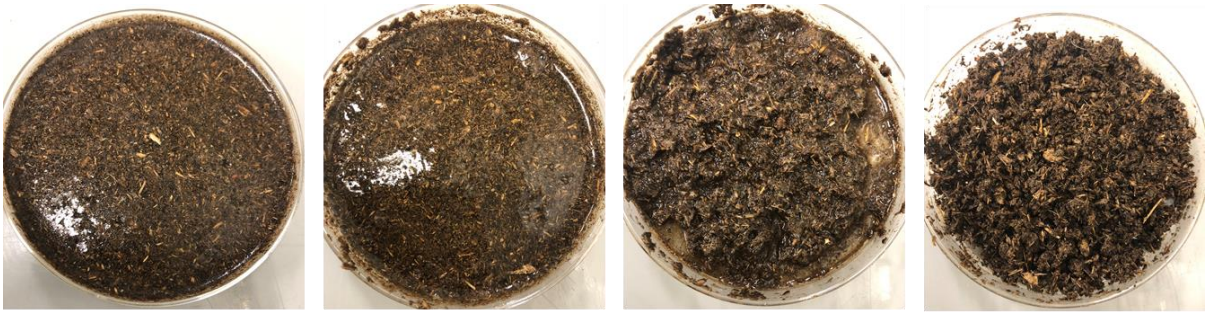

B/W=0.1 B/W=0.18 B/W=0.25 B/W=0.43

B/W=0.67 B/W=1.0

Appendix A: The prepared raw feedstocks of the DM at the different B/W ratios

Appendix B: The prepared raw feedstocks for the co-HTC process

Appendix C: The HTC reactor used for the study

Hydrochar from DM 200 °C

Hydrochar from DM 230 °C

Hydrochar from DM 255 °C

Hydrochar from DM 270 °C

Appendix D: Some produced hydrochar samples from dairy manure (DM)

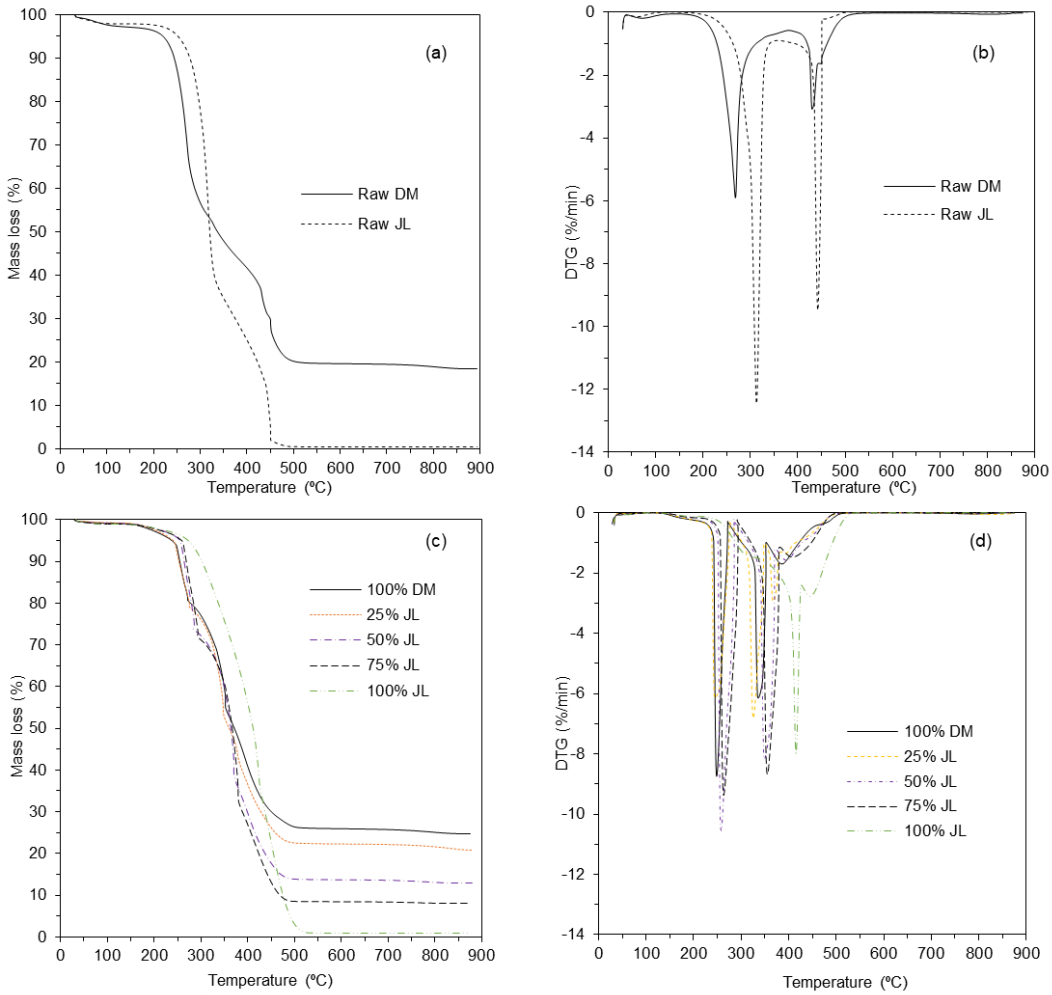

Appendix E: mass loss and the derivative at 5 °C/min

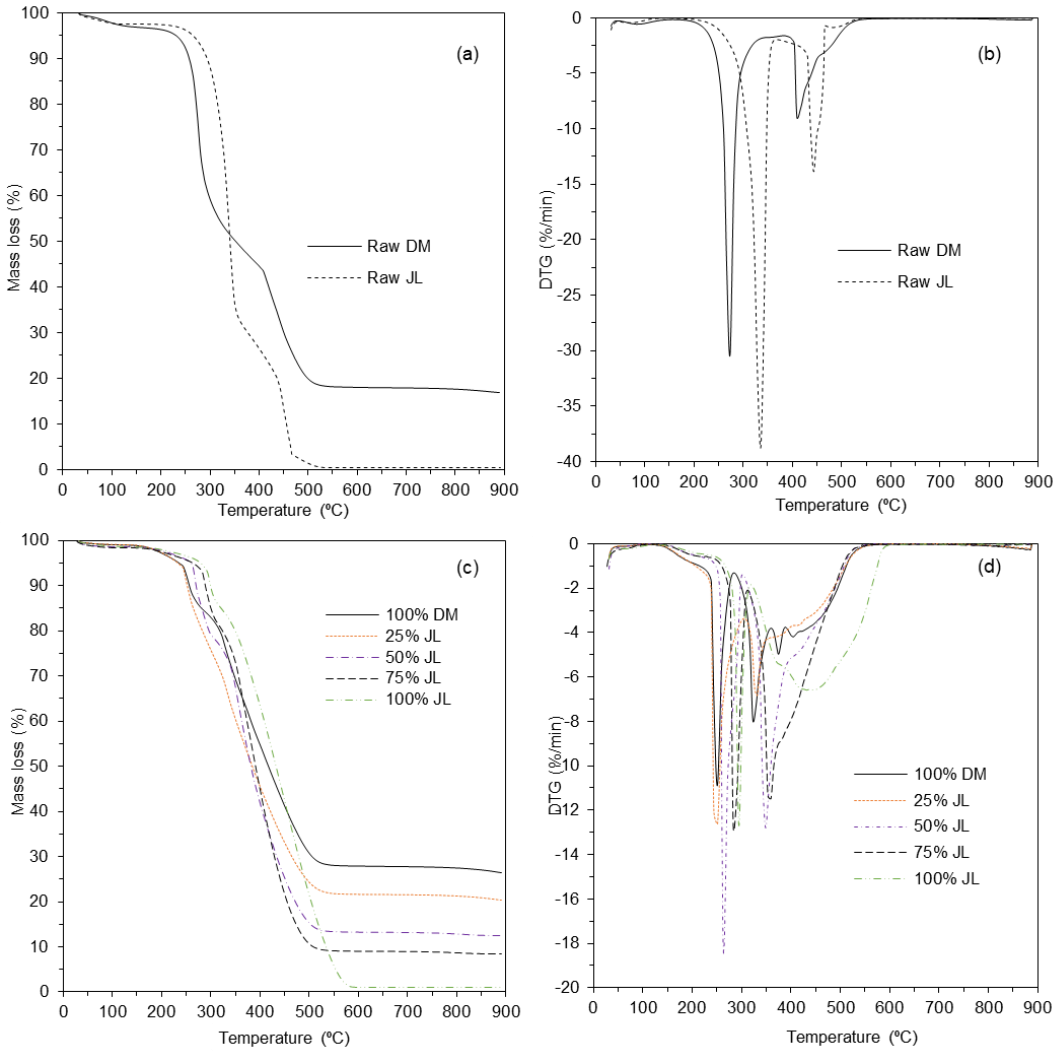

Appendix F: mass loss and the derivative at 15 °C/min

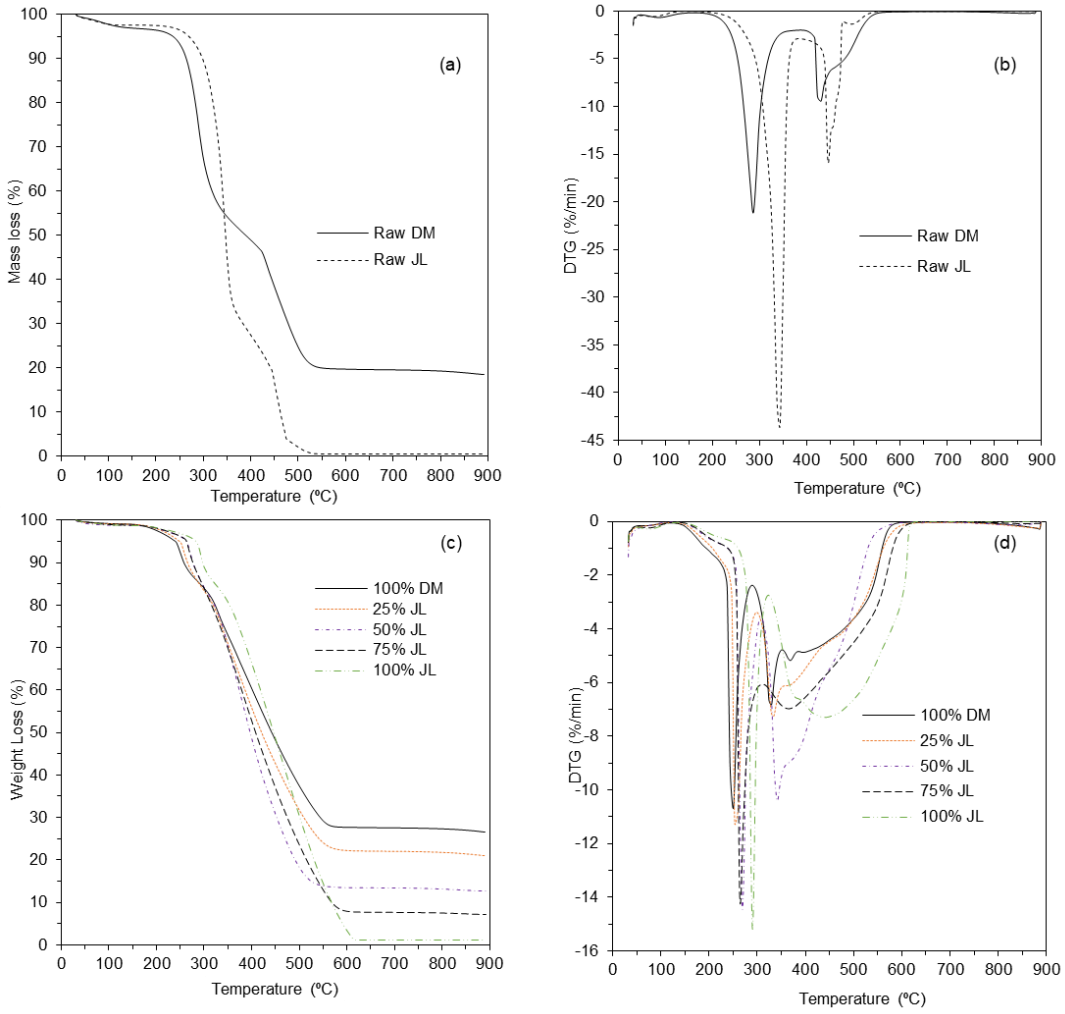

Appendix G: mass loss and the derivative at 20 °C/min

Appendix H: Derived equations at each conversion rate for FWO method

Raw DM		
Conversion	Equation	R^2
0.1	y = -5558.9x + 24.812	0.995
0.2	y = -5520.8x + 23.173	0.896
0.3	y = -8139.9x + 32.097	0.861
0.4	y = -5869.6x + 22.789	0.83
0.5	y = -7655.8x + 27.844	0.943
0.6	y = -3380.1x + 12.068	0.93
0.7	y = -4981.3x + 14.492	0.939
0.8	y = -10040x + 24.951	0.918

Raw JL		
Conversion	Equation	R^2
0.1	y = -4733.5x + 18.874	0.989
0.2	y = -5038.4x + 18.737	0.986
0.3	y = -6372.4x + 22.295	0.995
0.4	y = -6459.5x + 22.198	0.955

0.5	y = -5044.8x + 17.425	0.987
0.6	y = -5796.7x + 19.334	0.971
0.7	y = -24360x + 66.93	0.998
0.8	y = -15194x + 37.711	0.958

25% JL

Conversion	Equation	R^2
0.1	y = -2663.7x + 12.524	0.883
0.2	y = -3555.9x + 14.922	0.903
0.3	y = -5108.6x + 18.693	0.941
0.4	y = -4599.7x + 15.776	0.911
0.5	y = -4687.8x + 15.254	0.898
0.6	y = -3355x + 11.191	0.943
0.7	y = -4071x + 12.471	0.939
0.8	y = -4024.4x + 11.793	0.959

50% JL

Conversion	Equation	R^2
0.1	y = -4858.6x + 20.504	0.989
0.2	y = -10702x + 36.222	0.908
0.3	y = -4932.1x + 16.833	0.926
0.4	y = -8948.7x + 27.328	0.969
0.5	y = -9687.1x + 28.533	0.917
0.6	y = -7081.1x + 20.901	0.974
0.7	y = -4541.4x + 13.821	0.969
0.8	y = -5106.9x + 14.575	0.954

75% JL

Conversion	Equation	R^2
0.1	y = -3542.9x + 15.42	0.998
0.2	y = -3069.8x + 12.3	0.921
0.3	y = -3333.3x + 11.9	0.909
0.4	y = -4631.6x + 15.021	0.926
0.5	y = -4600x + 14.13	0.962
0.6	y = -4600x + 13.67	0.962
0.7	y = -4600x + 13.21	0.962
0.8	y = -4600x + 12.75	0.962

100% DM

Conversion	Equation	R^2
0.1	y = -4984.1x + 21.711	0.928
0.2	y = -3936.6x + 16.668	0.959
0.3	y = -3867x + 14.583	0.903
0.4	y = -5565.8x + 18.493	0.975
0.5	y = -4388.2x + 14.446	0.959
0.6	y = -3181.9x + 10.654	0.994
0.7	y = -3456.4x + 10.828	0.989
0.8	y = -3487.4x + 10.357	0.963

100% JL

Conversion	Equation	R^2
0.1	y = -5359.2x + 19.602	0.979
0.2	y = -4741.1x + 15.916	0.954

0.3	y = -6376.1x + 19.16	0.996
0.4	y = -6181.8x + 17.7	0.955
0.5	y = -7571.6x + 20.103	0.952
0.6	y = -6042.2x + 15.919	0.995
0.7	y = -5049.5x + 13.224	0.995
0.8	y = -4501x + 11.608	0.986

Appendix I: Derived equations at each conversion rate for KAS method

Raw DM

Conversion	Equation	R^2
0.1	y = -5026.5x + 11.642	0.995
0.2	y = -4939.7x + 9.8245	0.872
0.3	y = -7509.1x + 18.573	0.838
0.4	y = -5231.1x + 9.2495	0.792
0.5	y = -6985.4x + 14.206	0.929
0.6	y = -2651.1x - 1.7301	0.886
0.7	y = -4129.4x + 0.3846	0.913
0.8	y = -9057.5x + 10.55	0.898

Raw JL

Conversion	Equation	R^2
0.1	y = -4128.7x + 5.4506	0.987
0.2	y = -4389.9x + 5.1741	0.981
0.3	y = -5685.3x + 8.6146	0.992
0.4	y = -5759.8x + 8.4819	0.992
0.5	y = -4341.5x + 3.7007	0.983
0.6	y = -5073.1x + 5.5515	0.963
0.7	y = -23437x + 52.62	0.998
0.8	y = -14201x + 23.279	0.949

25% JL

Conversion	Equation	R^2
0.1	y = -2128.5x - 0.6532	0.829
0.2	y = -2975.4x + 1.5825	0.87
0.3	y = -4451.2x + 5.103	0.925
0.4	y = -3879.9x + 2.0045	0.877
0.5	y = -3936.2x + 1.3976	0.862
0.6	y = -2576.2x - 2.7383	0.906
0.7	y = -3236.7x - 1.5951	0.903
0.8	y = -3139x - 2.3928	0.931

50% JL

Conversion	Equation	R^2
0.1	y = -4291.2x + 7.2079	0.987
0.2	y = -9996.8x + 22.484	0.897
0.3	y = -4225.8x + 3.1005	0.905
0.4	y = -8160.3x + 13.369	0.961
0.5	y = -8888.4x + 14.551	0.906
0.6	y = -6267.6x + 6.8839	0.966
0.7	y = -3726.1x - 0.1985	0.957
0.8	y = -4231.6x + 0.4123	0.931

75% JL

Conversion	Equation	R^2
0.1	y = -3772.4x + 5.2698	0.987

0.2	y = -2244.1x - 1.8357	0.904
0.3	y = -4292.5x + 3.3002	0.859
0.4	y = -4042.6x + 1.7354	0.977
0.5	y = -4060x + 1.0196	0.971
0.6	y = -4080.4x + 0.5789	0.986
0.7	y = -3296.9x - 1.7729	0.962
0.8	y = -2873.7x - 3.1744	0.869

100% DM

Conversion	Equation	R^2
0.1	y = -4432.6x + 8.4702	0.909
0.2	y = -3356.1x + 3.3263	0.942
0.3	y = -3215.5x + 1.0123	0.868
0.4	y = -4836.3x + 4.695	0.966
0.5	y = -3623.8x + 0.5537	0.938
0.6	y = -2392.7x - 3.3026	0.986
0.7	y = -2613.4x - 3.26	0.977
0.8	y = -2580.3x - 3.8782	0.928

100% JL

Conversion	Equation	R^2
0.1	y = -4707x + 6.0279	0.975
0.2	y = -3998.5x + 2.0811	0.933
0.3	y = -5573.8x + 5.1711	0.994
0.4	y = -6848.1x + 7.2232	0.979
0.5	y = -6664.5x + 5.8686	0.939
0.6	y = -5107.9x + 1.6263	0.992
0.7	y = -4084.5x - 1.1333	0.989
0.8	y = -3492.4x - 2.8388	0.975